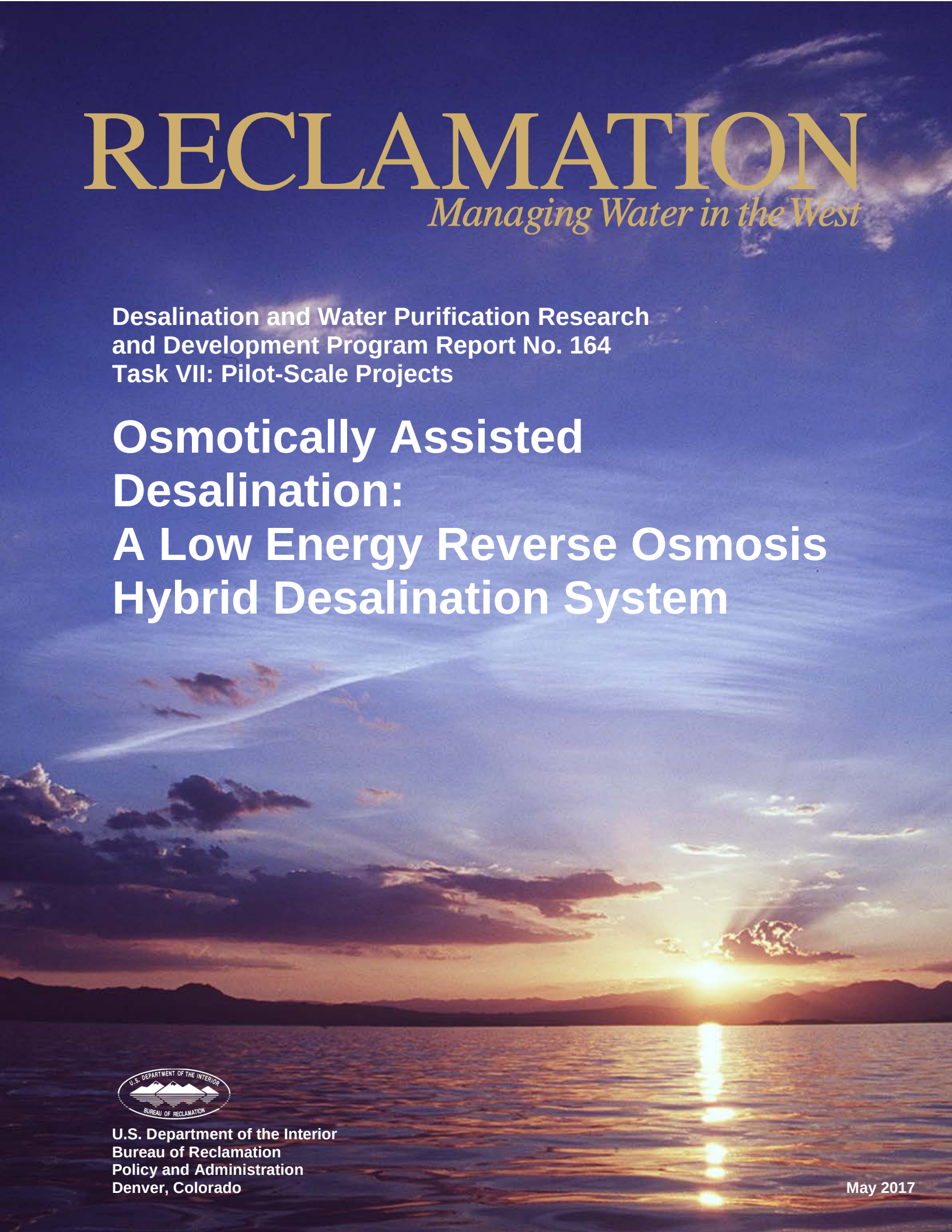

RECLAMATION

Managing Water in the West

Desalination and Water Purification Research and Development Program Report No. 164
Task VII: Pilot-Scale Projects

Osmotically Assisted Desalination: A Low Energy Reverse Osmosis Hybrid Desalination System

U.S. Department of the Interior
Bureau of Reclamation
Policy and Administration
Denver, Colorado

May 2017

REPORT DOCUMENTATION PAGE	*Form Approved OMB No. 0704-0188*

PLEASE DO NOT RETURN YOUR FORM TO THE ABOVE ADDRESS.

1. REPORT DATE *(DD-MM-YYYY)*	**2. REPORT TYPE**	**3. DATES COVERED** *(From - To)*
May 2017	Final	

4. TITLE AND SUBTITLE
Osmotically Assisted Desalination: A Low Energy Reverse Osmosis Hybrid Desalination System

5a. CONTRACT NUMBER
Agreement No. R10SF80251

5b. GRANT NUMBER

5c. PROGRAM ELEMENT NUMBER

6. AUTHOR(S)
Amy E. Childress

5d. PROJECT NUMBER

5e. TASK NUMBER

5f. WORK UNIT NUMBER

7. PERFORMING ORGANIZATION NAME(S) AND ADDRESS(ES)
University of Southern California
3260 South Vermont Ave, KAP 210
Los Angeles, CA 90089-2531

8. PERFORMING ORGANIZATION REPORT NUMBER

9. SPONSORING/MONITORING AGENCY NAME(S) AND ADDRESS(ES)
Desalination and Water Purification Research and Development Program
Bureau of Reclamation
Denver Federal Center
PO Box 25007
Denver CO 80225-0007

10. SPONSOR/MONITOR'S ACRONYM(S)
DWPR

11. SPONSOR/MONITOR'S REPORT NUMBER(S)
DWPR Report No. 164

12. DISTRIBUTION/AVAILABILITY STATEMENT
The following report provides a completed summary of the activity on the project to construct and test a reverse osmosis-pressure retarded osmosis (RO-PRO) pilot system. At this time all tasks are completed, and final results are included.

13. SUPPLEMENTARY NOTE

14. ABSTRACT
Pressure retarded osmosis (PRO) utilizes the chemical potential energy between streams of different salinity to generate power. PRO coupled with seawater reverse osmosis (RO) can be used to reduce the energy requirement, and therefore cost, of seawater desalination. In this project, the feasibility of the RO-PRO system was evaluated by model and experimental results. Modeling was conducted to determine the RO-PRO performance with cellulose triacetate (CTA) membranes and with virtual future-generation membranes, to test and evaluate the novel RO-PRO system (the first operating PRO pilot system in the United States), and to report the preliminary experimental results. The data collected from the pilot system testing was used to project the energy requirements of the components of the RO-PRO small pilot system and also to predict the results for a larger, optimized system. The results of this project can be used to better understand the relationship between freshwater production and power consumption using the RO-PRO system.

15. SUBJECT TERMS
Desalination, forward osmosis, pressure retarded osmosis, reverse osmosis, seawater, hybrid system, RO-PRO, energy recovery

16. SECURITY CLASSIFICATION OF:			**17. LIMITATION OF ABSTRACT**	**18. NUMBER OF PAGES**	**19a. NAME OF RESPONSIBLE PERSON**
a. REPORT	**b. ABSTRACT**	**a. THIS PAGE**		60	Katie Guerra
					19b. TELEPHONE NUMBER *(Include area code)* 303-445-2013

Desalination and Water Purification Research and Development Program Report No. 164
Task VII: Pilot-Scale Projects

Osmotically Assisted Desalination: A Low Energy Reverse Osmosis Hybrid Desalination System

Prepared for the Bureau of Reclamation
Under Agreement No. R10SF80251

by

Principal investigator

Amy E. Childress, Professor

Previously: Department of Civil & Environmental Engineering
University of Nevada, Reno
Currently: Sonny Astani Department of Civil & Environmental Engineering
University of Southern California
3260 South Vermont Ave; KAP 210
Los Angeles, CA 90089-2531
Email: amyec@usc.edu

U.S. Department of the Interior
Bureau of Reclamation

May 2017

MISSION STATEMENTS

The U.S. Department of the Interior protects America's natural resources and heritage, honors our cultures and tribal communities, and supplies the energy to power our future.

The mission of the Bureau of Reclamation is to manage, develop, and protect water and related resources in an environmentally and economically sound manner in the interest of the American public.

Disclaimer

The views, analyses, recommendations, and conclusions in this report are those of the authors and do not represent official or unofficial policies or opinions of the U.S. Government, and the United States takes no position with regard to any findings, conclusions, or recommendations made. As such, mention of trade names or commercial products does not constitute their endorsement by the U.S. Government.

ACRONYMS AND ABBREVIATIONS

CA	California
CO	Colorado
CTA	cellulose triacetate
Eq.	equation
ERD	energy recovery devices
FO	forward osmosis
g/L	gallons per liter
HTI	Hydration Technology Innovations
IL	Illinois
kPa	kilopascal
kWh/m^3	kilowatt/meter
LPM	liters per minute
m	meter
m^3/d	meter per day
MA	Massachusetts
MI	Michigan
mm^{-1}	milometers
MN	Minneapolis
m/s	meter per second
NaCl	sodium chloride
NJ	New Jersey
NM	New Mexico
NY	New York
OR	Oregon
PRO	pressure-retarded osmosis
psi	pounds per square inch
PX	pressure exchanger
Reclamation	Bureau of Reclamation
RO	reverse osmosis
U.S.	United States
VA	Virginia
W/m^2	Watts per square meter

CONTENTS

Page

APPENDICES

TABLES

FIGURES

1. INTRODUCTION

With growing concerns about the rising costs and environmental consequences of fossil fuels, renewable resources are becoming increasingly important. While solar and wind are among the most well-known renewable resources, another nearly untapped resource lies in estuaries where rivers meet seas. This salinity gradient power potential is significant as it could increase current renewable energy production by up to 20 percent [1, 2]. One way to harvest salinity gradient power is through pressure-retarded osmosis (PRO). Similar to forward osmosis (FO) and reverse osmosis (RO), PRO utilizes a semi-permeable membrane which separates a high salinity solution from a low salinity solution. In FO, water permeates the membrane strictly due to osmosis; in RO, water permeates the membrane due to an applied hydraulic pressure that overcomes the osmotic pressure. Likewise, PRO utilizes a pressurized draw solution that does not overcome the osmotic pressure so that water still permeates the membrane and dilutes the high salinity solution. The chemical potential between the high and low salinity solutions is transformed into hydraulic pressure as water is transferred from the low salinity side to the pressurized high salinity solution side. This hydraulic pressure can be used to rotate a turbine and create power [3]. The idea of salinity gradient power was first introduced in the 1950s, but with little interest in pursuing renewable energy at that time, the next leap in PRO did not occur until the late 1970s and early 1980s [4-10] when different configurations of PRO were investigated. It was not until recently that research has begun focusing on enhancements that would facilitate future commercial production [11-22].

Open-loop PRO systems can take advantage of naturally occurring salinity gradients (e.g., in estuaries where the river meets the sea) in a “river-to-sea PRO” scenario (figure 1a). In these systems, the energy that is spent by the sun evaporating water from the sea is recovered by a PRO system that captures the energy in the estuary where the river water mixes with the seawater. Open-loop systems can also be used with engineered salinity gradients (e.g., in the disposal/dilution of the concentrate stream at RO membrane facilities) in a “RO-PRO” scenario (figure 1b). Closed-loop PRO systems are designed to convert low-grade (“waste”) heat into mechanical work (figure 1c). RO-PRO (osmotic pump) systems and closed-loop (osmotic heat engine) systems are considered to be sustainable energy systems.

RO desalination is currently the most efficient desalination technology; however, it still requires a great deal of energy to create the high pressures necessary to overcome the osmotic pressure of saline waters [23, 24]. RO desalination energy consumption ranges from 6 to 8 kWh/m^3 without the use of energy recovery devices (ERDs) [23]. However, with efficiencies up to 97 percent, ERDs are now commonplace and can reduce energy consumption by as much as 60 percent [25].

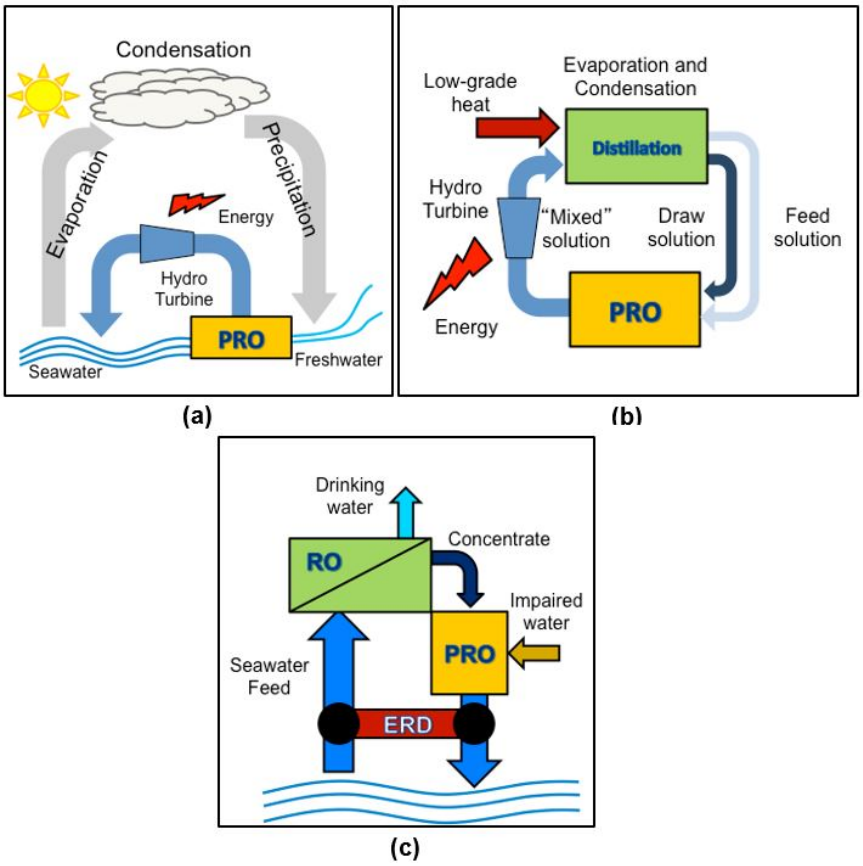

Figure 1.—(a) Diagram of an open-loop PRO configuration to recover chemical potential energy, (b) diagram of a closed-loop, or osmotic heat engine) PRO configuration to convert low grade waste-heat into mechanical work, and (c) diagram of RO-PRO configuration where PRO recovers the chemical potential energy between RO brine and an impaired freshwater source.

In fact, implementing an ERD such as a pressure exchanger (PX) has shown to decrease desalination energy consumption to less than 2.5 kWh/m^3 in RO-PX systems [26]. Also, by including an ERD, the size of the RO high pressure pump can be reduced for the same design capacity, and a smaller, more efficient pump can be selected [27]. In addition to energy costs for seawater desalination, there are also environmental concerns associated with the discharge of concentrated brine through ocean outfalls [28]. If a seawater desalination facility has a recovery of 40-50 percent, then 50-60 percent of the intake seawater becomes concentrated brine. Some of the concerns with discharging brines to the ocean include high salinity plumes in receiving waters at desalination outfalls and the spread of contaminants in receiving waters due to use of anti-scalants and anti-foulants [29]. For these reasons, the effects of concentrated brine on the marine environment have been negatively reported in the literature [30-35]. Considering that the worldwide production of fresh drinking water from desalination plants is around 24.5 million m^3/d with new desalination projects in progress, a solution to the discharge of concentrated brines would have wide application.

Figure 2 is a diagram of the RO-PRO system whereby seawater or another high salinity feed solution (V_f) is pre-pressurized in the PX prior to entering the RO sub-system where desalination occurs. Two streams exit the RO sub-system: a freshwater permeate stream ($V_{p,RO}$) and a concentrated brine waste stream (V_b). The concentrated brine stream enters the PRO sub-system as a high salinity (draw) solution ($V_{ds,en}$). The feed solution for the PRO sub-system ($V_{f,en}$) is a low salinity solution. Through osmosis, the pressurized draw solution extracts water from the impaired water source under isobaric conditions, resulting in a diluted draw solution ($V_{ds,ex}$). The energy stored in the diluted draw solution is exchanged with the seawater RO feed prior to discharge in order to recover its potential energy and increase the energy savings of the RO-PRO system.

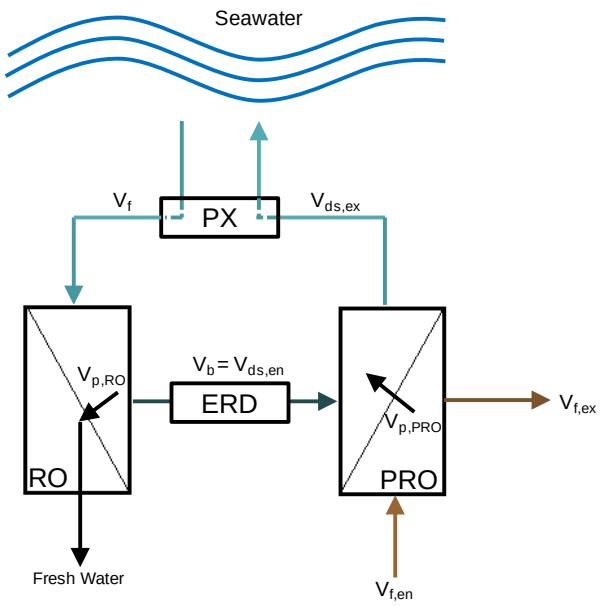

Figure 2.—Diagram of the RO-PRO system where the RO feed solution (V_f) is pre-pressurized in the PX prior to entering the RO sub-system where desalination occurs. Exiting the RO sub-system are two streams: a freshwater permeate stream ($V_{p,RO}$) and a concentrated brine waste stream (V_b). The concentrated RO brine stream (V_b) is first partially depressurized using an ERD and then enters the PRO sub-system as the draw solution ($V_{ds,en}$). The feed solution for the PRO sub-system ($V_{f,en}$) is a low salinity solution. Through osmosis, the pressurized draw solution extracts water from the impaired water source under isobaric conditions, resulting in a concentrated feed ($V_{f,ex}$) and diluted draw solution ($V_{ds,ex}$). The energy stored in the diluted draw solution is exchanged with the seawater RO feed in the PX prior to discharge in order to recover its potential energy and increase the energy savings of the RO-PRO system.

The RO-PRO system has numerous advantages. Compared to RO-PX systems, RO energy consumption is further reduced with energy production by PRO. Another key advantage of this system is that the brine generated during the RO process is diluted back to seawater concentration. From a PRO perspective, simply disposing RO brine to the sea is a waste of a “good” draw solution. Thus, a

PRO system that uses concentrated brine as a draw solution not only reduces feedwater pumping requirements but minimizes the adverse environmental impact on marine ecology/habitats that can occur during seawater RO brine disposal.

Only two RO-PRO pilot systems have been reported in the literature. A prototype plant in Japan utilizes the concentrated brine stream from a local RO plant as the draw solution and treated sewage as the impaired water source. Eight ten-inch hollow fiber membrane modules are being tested and membrane fouling has been the major problem encountered in this system [36]. In the United States (U.S.), through funding from the Bureau of Reclamation (Reclamation), a pilot-scale RO-PRO system has been designed and constructed [37] and is currently being tested in the laboratory using simulated seawater and tap water as a surrogate impaired water source. Using tap water instead of a wastewater avoids the fouling issues that have afflicted previous systems so that the maximum potential of the RO-PRO system can be assessed. The research is focused on achieving pilot results that will verify the approximate 30 percent reduction in specific energy consumption theoretically predicted for the RO-PRO system compared to an optimized RO system (i.e., RO with an energy recovery device) [38].

In this project, the feasibility of the RO-PRO system was evaluated by model and experimental results. The specific objectives were to model RO-PRO performance with cellulose triacetate (CTA) membranes and virtual future generation membranes, to present the novel RO-PRO system (the first operating PRO pilot system in the United States), and to report the preliminary experimental results focused on the relationship between freshwater production and power consumption. To accomplish the modeling objectives, the energetics of each sub-system were first evaluated separately. The minimum RO specific energy consumption was determined considering RO at its thermodynamic limit and utilizing models from the literature [39]. The PRO specific energy production was calculated utilizing a new PRO model, which takes into account membrane characteristics, water flux, reverse salt flux, concentration polarization effects, and pressure drops in the membrane module. The PRO model, combined with the RO model, was then used to provide a theoretical specific energy requirement for the RO-PRO system. This specific energy requirement was compared to the energy requirements of an ideal RO-PRO system and an optimized RO system. Then, sensitivity analyses were performed to gain insight into major areas of development needed to improve the energy reduction achievable by the RO-PRO system. To accomplish the experimental objectives, the concentrated brine from the RO sub-system was used as the high salinity draw solution and tap water was used as the low salinity feed water in the PRO sub-system. The data collected from the pilot system testing was then used to project the energy requirements of the components of the RO-PRO small pilot system and also to predict the results for a larger, optimized system.

2. THEORY AND MODEL DEVELOPMENT

2.1 Theory

2.1.1 Thermodynamically Reversible RO Desalination

In figure 3a, a volume of feed solution (V_f) (e.g., seawater) enters the system under a high hydraulic pressure and is separated into a relatively pure permeate ($V_{p,RO}$) and a concentrated brine (V_b).

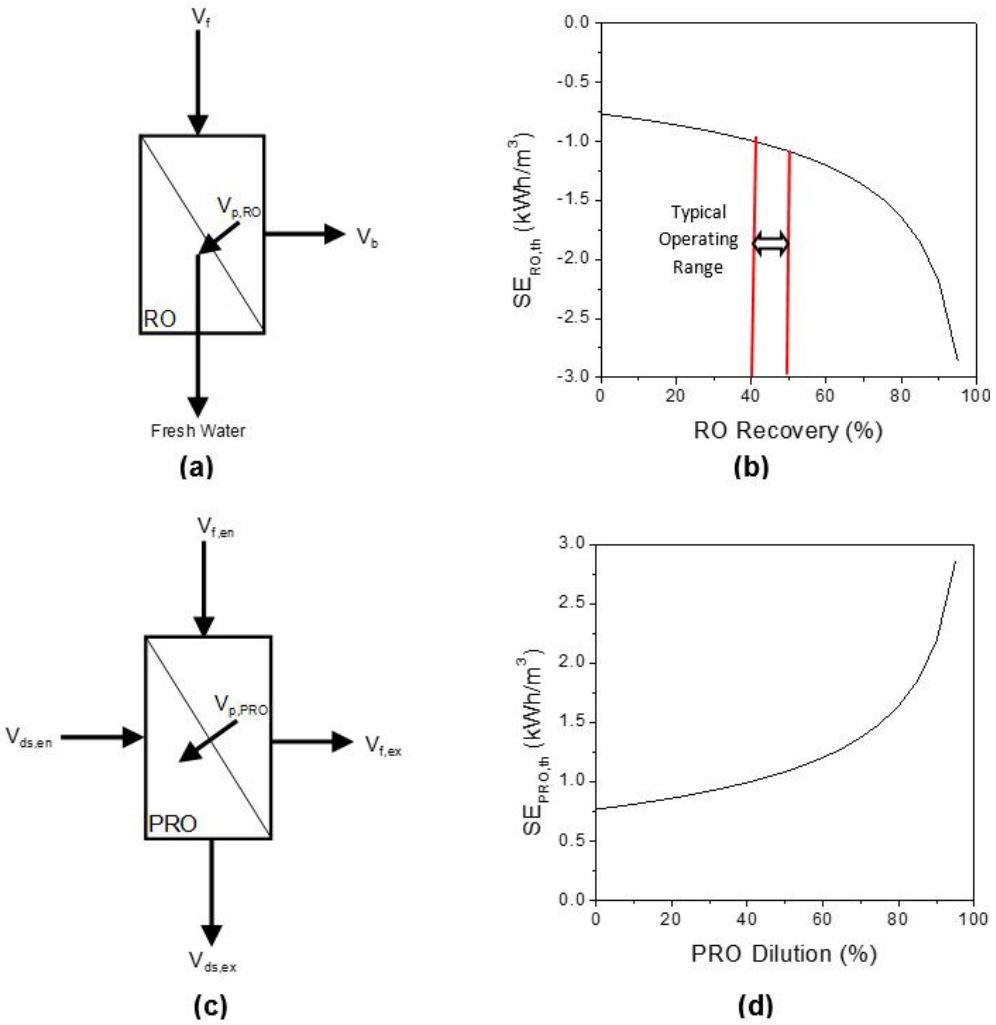

Figure 3.—(a) RO flow diagram and (b) ideal RO specific energy consumption for freshwater recovery in RO. (c) PRO flow diagram and (d) ideal PRO specific energy production for draw solution dilution to seawater in PRO. For RO, subscripts *f*, *b*, and *p,RO* indicate feed, brine, and RO permeate, respectively. For PRO, subscripts *f*, *ds*, and *p,PRO* indicate PRO feed, draw solution, and permeate, respectively, and *en* and *ex* indicate entering and exiting, respectively.

The energy requirement of a thermodynamically reversible (i.e., ideal) RO desalination process can be determined through manipulation of mass and energy balance equations. Assuming finite recovery in an ideal desalination process, the energy requirement can be calculated based on the mole fraction of the feed and brine solutions utilizing the work equation [40]:

$$W_{th,RO} = iRT \frac{X_b X_f}{(X_b - X_f)} ln\left(\frac{X_b}{X_f}\right) \quad (1)$$

where $W_{th,RO}$ is the ideal work per volume of RO permeate (i.e., volume of freshwater produced), i is the van't Hoff factor, R is the universal gas constant, T is the constant temperature of the feed and brine solutions, and X is the salt mole fraction with the subscripts f and b indicating the feed and brine solutions, respectively. For the purposes of this project, osmotic pressure is a preferable term over mole fraction. Each mole fraction (X) in equation (Eq.) (1) is replaced with molarity (M), which is in turn converted into osmotic pressure using the Morse Equation:

$$\pi = \frac{M}{iRT} \quad (2)$$

where π is osmotic pressure. This results in the following equation for the ideal specific work, or ideal specific energy ($SE_{RO,th}$) consumption for RO separation:

$$SE_{RO,th} = \left(\frac{\pi_b \pi_f}{\pi_b - \pi_f}\right) ln\left(\frac{\pi_b}{\pi_f}\right) \quad (3)$$

which gives the specific energy consumption per volume of freshwater produced.

In order to determine osmotic pressures for given molar concentrations of salts, which are dependent on the van't Hoff factor, OLI Stream Analyzer 2.0 software (OLI Systems, Inc., Morris Plains, NJ) was used. For example, OLI data give the following relationship between osmotic pressure (in kPa) and molarity for sodium chloride (NaCl):

$$\pi_{NaCl} = 351.15 {M_{NaCl}}^2 + 4365.18 M_{NaCl} + 25.72 \quad (4)$$

In figure 3b, the $SE_{RO,th}$ (with energy consumption indicated by a negative specific energy) is shown as a function of the recovery of pure water from a 3.5 percent salinity solution (i.e., seawater). Recovery (Y) of the RO system is given by:

$$Y = \frac{V_{p,RO}}{V_f} \quad (5)$$

where V is volume. The subscript p,RO represents RO permeate. As seen in figure 3b, at zero recovery, the $SE_{RO,th}$ consumption is approximately 0.77 kWh

per m^3 of freshwater produced. This is the energy required to produce a drop of freshwater from an infinite pool of seawater. As recovery increases, the $SE_{RO,th}$ consumption also increases, indicating the tradeoff between freshwater recovery and energy costs associated with an RO system. Typically, the optimal recovery rate for a seawater RO system is in the range of 40-50 percent and in this case, the $SE_{RO,th}$ consumption would be approximately 1.0-1.1 kWh/m^3. However, actual desalination energy consumption is larger because a desalination facility is finite in size and thus does not operate as a reversible thermodynamic process [41]. For example, the Ashkelon facility in Israel, one of the most efficient seawater RO desalination facilities, operates at approximately 40 percent recovery and has a maximum nominal electrical *SE* consumption of 3.9 kWh/m^3 [42, 43].

2.1.2 Thermodynamically Reversible PRO Mixing

Figure 3c is a diagram of the PRO process where, similar to RO, a portion of the feed stream permeates through a semi-permeable membrane [44]. In a PRO system, the feed solution ($V_{f,en}$) enters the system under atmospheric pressure and through osmosis, relatively pure water ($V_{p,PRO}$) permeates through the membrane into a pressurized high salinity draw solution ($V_{ds,en}$) that exits as a diluted draw solution ($V_{ds,ex}$). The rejected feed solution ($V_{f,ex}$) exits as a more concentrated solution.

For PRO, an equation similar to Eq. (1) can be developed. Assuming finite dilution in an ideal mixing process, the energy production can be calculated utilizing:

$$W_{th,PRO} = iRT \frac{X_{ds,en}X_{ds,ex}}{\left(X_{ds,en} - X_{ds,ex}\right)} ln\left(\frac{X_{ds,ex}}{X_{ds,en}}\right) \tag{6}$$

where $W_{th,PRO}$ is the ideal work per volume of PRO permeate. The subscripts *ds,en* and *ds,ex* indicate the entering draw solution and exiting draw solution, respectively. Following the same steps as described for RO separation (Eqs. 1 through 3), the resulting equation for the ideal specific energy ($SE_{PRO,th}$) production for PRO mixing is:

$$SE_{PRO,th} = \left(\frac{\pi_{ds,en}\pi_{ds,ex}}{\pi_{ds,en} - \pi_{ds,ex}}\right) ln\left(\frac{\pi_{ds,ex}}{\pi_{ds,en}}\right) \tag{7}$$

which gives the specific energy production per volume of PRO permeate. The osmotic pressure of the exiting draw solution can be found after determining the permeate volume for a predetermined PRO dilution (*D*), which is defined as:

$$D = \frac{V_{p,PRO}}{V_{ds,ex}} \tag{8}$$

where the subscript *p,PRO* represents PRO permeate. *D* is purposely defined to express the PRO permeate over the total exiting volume of draw solution ($V_{ds,en}$ + $V_{p,PRO}$) to maintain consistency with *Y* (the RO permeate volume over the total RO feed volume (V_b + $V_{p,RO}$). In figure 3d, the $SE_{PRO,th}$ production is shown as a function of the dilution of a RO brine to a 3.5 percent salinity solution (i.e., seawater). As seen in figure 3d, the minimum ideal $SE_{PRO,th}$ is approximately 0.77 kWh/m^3 and is achieved when $D = 0$, or when $C_{ds,en} = C_{ds,ex}$. As dilution increases, the $SE_{PRO,th}$ production also increases and mirrors the $SE_{RO,th}$ consumption curve. Thus, more specific energy can be extracted when the dilution is higher. A higher dilution can be achieved with a higher entering draw solution concentration.

2.1.3 Thermodynamically Reversible RO-PRO System

The thermodynamically reversible RO-PRO system is evaluated by combining the ideal RO and PRO processes. The ideal net specific energy ($SE_{net,th}$) of the RO-PRO system as a function of PRO dilution for RO recoveries between 30 and 60 percent is given in figure 4. $SE_{net,th}$ is defined as the energy required (or energy produced) per unit volume of RO permeate. The $SE_{net,th}$ is negative when the RO-PRO system consumes energy and positive when the RO-PRO system produces energy. In figure 4, the maximum $SE_{net,th}$ consumption values, which occur when there is no contribution from the PRO sub-system (dilution = 0), are -0.92, -0.99, -1.08, and -1.20 kWh/m^3 for 30, 40, 50, and 60 percent RO recoveries, respectively. These values correspond to the ideal RO energy consumption values given in figure 3b. As dilution increases and PRO begins producing energy, the RO-PRO system specific energy consumption decreases. For each RO recovery, the specific energy reaches zero when the PRO dilution is equal to the RO recovery, or when the exiting PRO draw solution volume is equal to the RO feed solution volume. This point represents an ideal energy neutral system where the energy consumed by RO is offset by the energy produced by PRO. As PRO dilution increases past the energetically neutral point, the RO-PRO system begins producing energy. It can be seen that, the RO-PRO system $SE_{net,th}$ production is greater for lower RO recoveries. This is because the $SE_{net,th}$ is normalized to the RO permeate flowrate, which is lower for lower RO recoveries and results in a greater $SE_{net,th}$ production. However, this should not imply that RO-PRO system operation at low RO recovery is desirable. For instance, the $SE_{PRO,th}$ (data not shown) for a *D* of 50 percent and RO recoveries of 30, 40, 50, and 60 percent are 0.76, 0.90, 1.08, and 1.38 kWh/m^3, respectively, showing that the productivity of PRO is greater for higher RO recoveries. Thus, a tradeoff between energy and membrane area (i.e., capital and operating costs) must be considered.

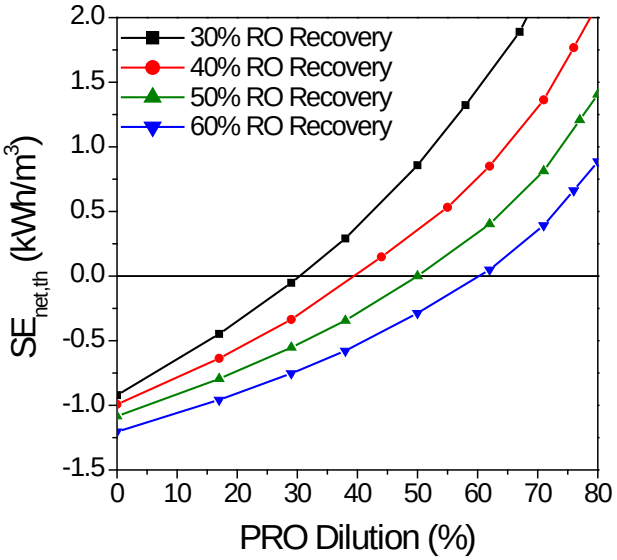

Figure 4.—Net ideal RO-PRO specific energy ($SE_{net,th}$) as a function of PRO dilution (D) with RO recoveries between 30 and 60 percent.

Compared to an ideal RO-PRO system, an actual RO-PRO system will operate in the negative *SE* region only and not be a net energy producing system. Furthermore, in an actual system, the energy requirements are expected to be greater than the theoretical amounts and the energy productions are expected to be less than the theoretical amounts. When the draw solution is seawater and the feed solution is river water with a minimum possible (although unlikely) salinity of 0 percent [45], the minimum PRO energy production in RO-PRO (0.77 kWh/m^3) is the maximum PRO energy production in the river-to-sea configuration. It has been estimated that because PRO facilities will be finite in size and will not operate as thermodynamically reversible processes, the actual SE_{PRO} in the river-to-sea configuration would be approximately 0.3-0.4 kWh/m^3 with a 50 percent overall PRO efficiency [46].

2.2 Model Development

2.2.1 Thermodynamically Irreversible RO Desalination Model

The SE_{RO} consumption for the RO sub-system under real conditions at the thermodynamic restriction ($SE_{RO,tr}$) is defined as [39]:

$$SE_{RO,tr} = \frac{R * \pi_f}{\eta_p Y(1-Y)} \tag{9}$$

where R is the salt rejection and η_p is the pump efficiency. The thermodynamic restriction occurs at the lowest hydraulic pressure in which the RO system will produce freshwater. The hydraulic pressure must be greater than the exiting brine osmotic pressure in order for the RO system to produce a drop of freshwater.

Operating at the thermodynamic restriction gives the minimum energy requirement for the RO process. The $SE_{RO,tr}$ term is given in pressure units, which correspond to energy consumed per volume of freshwater produced.

ERDs, such as PXs or work exchangers, can recover pressure from the high-pressure concentrated brine stream that would otherwise be lost at seawater RO facilities. Equation (9) can be rewritten to account for the use of an ERD (i.e., optimized RO) [39]:

$$SE_{RO,tr}^{ERD} = \frac{\big(1 - \eta_E(1 - Y)\big)R * \pi_f}{\eta_p Y(1 - Y)} \tag{10}$$

where η_E is the efficiency of the ERD. Most devices have maximum efficiencies of 97 percent [25].

2.2.2 Thermodynamically Irreversible PRO Mixing Model

While a model for bench-scale PRO systems was previously established [47, 48], a model to evaluate the $SE_{PRO,th}$ production for full-scale PRO systems is not available. Therefore, a module-based PRO model was developed to account for the effects of water flux, reverse salt flux, concentration polarization, and pressure drops on the flowrates, concentrations, and pressures as the feed and draw solutions pass through the PRO membrane module.

Water flux (J_w) was evaluated using [8]:

$$J_W = A\big(\Delta\pi_{eff} - \Delta P_{net}\big) \tag{11}$$

where A is the water permeability coefficient, $\Delta\pi_{eff}$ is the effective osmotic pressure difference across the membrane, and ΔP_{net} is the net hydraulic pressure difference across the membrane.

Reverse salt flux, or the passage of salt from the draw solution through the membrane and into the feed solution, occurs in FO and PRO processes. It decreases the concentration of the draw solution and increases the concentration of the feed solution. Salt flux (J_s) can be determined by Fick's Law:

$$J_S = B\Delta C_{eff} \tag{12}$$

where B is the salt permeability coefficient and ΔC_{eff} is the effective difference between the salt concentrations on either side of the dense layer interface. $\Delta\pi_{eff}$ and ΔC_{eff} are both reduced by concentration polarization effects [47, 48]. Concentration polarization is a severe phenomenon that reduces the effective osmotic pressure difference across the membrane due to an accumulation or depletion of solutes near the interface [49]. As water crosses the membrane, solutes are concentrated on the feed side of the membrane surface and diluted on

the permeate side of the membrane surface. Significant research has already been presented on concentration polarization effects and supporting theory is available in the literature [47, 48].

Accounting for salt permeability and concentration polarization, $\Delta\pi_{eff}$ is given as [48]:

$$\Delta\pi_{eff} = \frac{\pi_{ds,b}\exp\left(-\frac{J_W}{k}\right) - \pi_{f,b}\exp(J_W K)}{1 + \frac{B}{J_W}\left[\exp(J_W K) - \exp\left(-\frac{J_W}{k}\right)\right]} \tag{13}$$

where K is the solute resistivity for diffusion within the porous support layer, k is the mass transfer coefficient in the draw solution, and π is the osmotic pressure with subscripts *ds* and *f* indicating the draw solution and the feed, respectively. Eq.11 becomes:

$$J_W = A\left(\frac{\pi_{ds,b}\exp\left(-\frac{J_W}{k}\right) - \pi_{f,b}\exp(J_W K)}{1 + \frac{B}{J_W}\left[\exp(J_W K) - \exp\left(-\frac{J_W}{k}\right)\right]} - \Delta P_{net}\right) \tag{14}$$

The net hydraulic pressure difference (ΔP_{net}) across the membrane is given as:

$$\Delta P_{net} = \left(P_{ds,en} - \Sigma P_{ds,loss}\right) - \left(P_{f,en} - \Sigma P_{f,loss}\right) = \Delta P - \Sigma P_{ds,loss} + \Sigma P_{f,loss} \tag{15}$$

where P is the pressure with the subscripts *en* and *loss* indicating entering and loss, respectively. ΔP is the pressure difference across the membrane. Thus, in order to determine ΔP_{net}, pressure drops through the membrane module in the feed and draw solution channels are calculated. Due to the turbulent nature of the flow, the solution pressure losses (P_{loss}) in spiral wound modules are accounted for by [50]:

$$P_{loss} = \frac{\lambda\rho v^2 L}{2d_h} \tag{16}$$

where ρ is the density of the solution, v is the cross flow velocity, L is the length of the module, d_h is the hydraulic diameter, and λ is the friction coefficient calculated by:

$$\lambda = 6.23Re^{-0.3} \tag{17}$$

The friction coefficient applies to all types of feed spacers and is valid for low Reynolds numbers ($100 < Re < 1000$), which can be calculated using:

$$Re = \frac{\rho v L}{\mu} \tag{18}$$

where μ is the dynamic viscosity. The dynamic viscosity and density of the solution were obtained using relationships from OLI Stream Analyzer 2.0.

Similar to the modification of $\Delta\pi$ to account for reverse salt flux and concentration polarization, ΔC_{eff} is given as [48]:

$$\Delta C_{eff} = \frac{C_{ds,b} \exp\left(-\frac{J_W}{k}\right) - C_{f,b}\exp(J_W K)}{1 + \frac{B}{J_W}\left[\exp(J_W K) - \exp\left(-\frac{J_W}{k}\right)\right]} \tag{19}$$

where C is the salt concentration, Eq (12) becomes:

$$J_S = B\left(\frac{C_{ds,b} \exp\left(-\frac{J_W}{k}\right) - C_{f,b}\exp(J_W K)}{1 + \frac{B}{J_W}\left[\exp(J_W K) - \exp\left(-\frac{J_W}{k}\right)\right]}\right) \tag{20}$$

To create a model for full-scale PRO applications, a theoretical spiral wound membrane was divided into incremental segments (dL) along its length to evaluate flow conditions at specific points in the membrane module. The first segment has known entering conditions and the exiting conditions can be calculated and will become the entering conditions for the next segment. This process is repeated until the end of the membrane module is reached. Figure 5 is a single segment of a membrane module where the exit flowrates, concentrations, and pressures of the draw and feed solutions can be determined using:

$$Q_{ds,out} = Q_{ds,in} + J_W A_{eff} \tag{21}$$

$$Q_{f,out} = Q_{f,in} - J_W A_{eff} \tag{22}$$

$$C_{ds,out} = \frac{Q_{ds,in}C_{ds,in} - J_S A_{eff}}{Q_{ds,in} + J_W A_{eff}} \tag{23}$$

$$C_{f,out} = \frac{Q_{f,in}C_{f,in} + J_S A_{eff}}{Q_{f,in} - J_W A_{eff}} \tag{24}$$

$$P_{ds,out} = P_{ds,in} - P_{ds,loss} \tag{25}$$

$$P_{f,out} = P_{f,in} - P_{f,loss} \tag{26}$$

where Q is flowrate and A_{eff} is the area of the increment calculated using dL and the width along the length of the segment. The subscripts *in* and *out* represent entering and exiting from the segment, respectively. In figure 5, the subscripts *m* and *b* represent membrane and bulk, respectively.

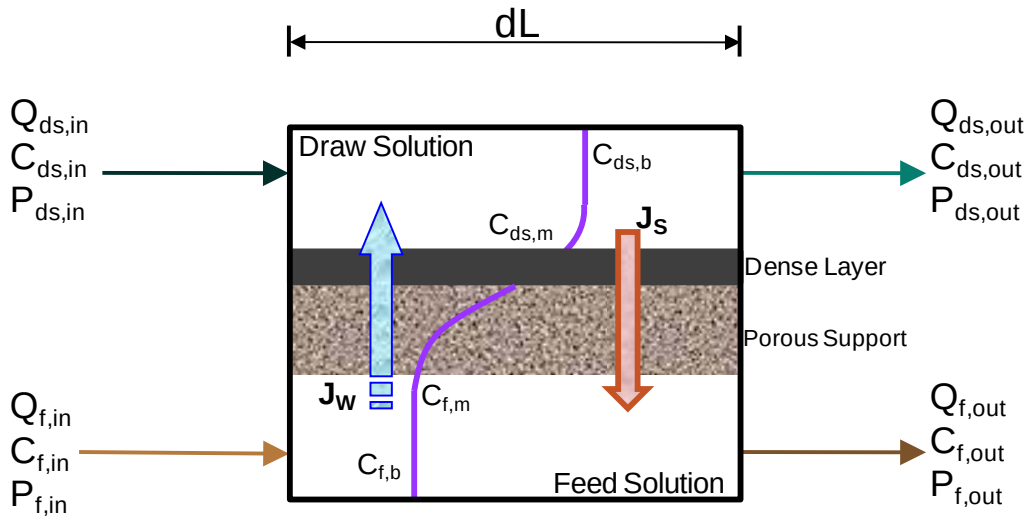

Figure 5.—A single segment (*dL*) along the length of a PRO membrane module. Variables Q, C, and P are flowrate, concentration, and pressure, respectively, while subscripts in, out, m, and b are entering condition, exiting condition, membrane, and bulk, respectively. J_w represents water flux (blue arrow), and J_s represents reverse salt flux (red arrow). Concentration polarization is represented by the purple line, which shows that the draw solution concentration decreases close to the membrane active layer and the feed solution increases in the membrane support layer.

The power density in PRO is equal to the product of the water flux through the membrane and the hydraulic pressure difference across the membrane considering pressure drops. Thus, power density (W) was calculated at the end of the membrane module or modules as:

$$W = \frac{Q_{Totalp,PRO}\Delta P_{net}}{A_{Total}} \tag{27}$$

where A_{Total} is the total membrane area and $Q_{Totalp,PRO}$ is the sum of the permeate flowrate for each segment in the model:

$$Q_{Totalp,PRO} = \sum J_w A_{eff} \tag{28}$$

In order to maximize power density, ΔP needs to be equal to $\Delta\pi_{eff}/2$ [47]. From Eq. 15, $\Delta P_{net,opt}$ then becomes:

$$\Delta P_{net,opt} = \frac{1}{2}\left(\frac{\pi_{ds,b}\exp\left(-\frac{J_{W,avg}}{k}\right) - \pi_{f,b}\exp\left(J_{W,avg}K\right)}{1 + \frac{B}{J_{W,avg}}\left[\exp\left(J_{W,avg}K\right) - \exp\left(-\frac{J_{W,avg}}{k}\right)\right]}\right) - \Sigma P_{ds,loss} + \Sigma P_{f,loss} \tag{29}$$

where $J_{W,avg}$ is the average water flux along the length of the membrane module.

Power density describes the power production per area of PRO membrane and allows for convenient comparison between membranes. Similar to the SE_{RO}, the SE_{PRO} is the energy production per volume of PRO permeate, or the power density per water flux. Therefore, the SE_{PRO} can be calculated by dividing Eq. (27) by $J_{W,avg}$ along the length of the membrane module, resulting in:

$$SE_{PRO} = \frac{Q_{Totalp,PRO}\Delta P_{net,opt}}{A_{Total}J_{W,avg}} \tag{30}$$

where the total PRO permeate flowrate divided by the total membrane area is the average water flux along the length of the membrane module. Therefore, a $J_{W,avg}$ term is also in the numerator, and $J_{W,avg}$ cancels out to result in:

$$SE_{PRO} = \Delta P_{net,opt} \tag{31}$$

Eq. (31) effectively links the SE_{PRO} to the operating pressure that maximizes power density.

2.2.3 Thermodynamically Irreversible RO-PRO System Model

The model RO-PRO system specific energy consumption can be evaluated combining the RO energy consumption at the thermodynamic limit with the modeled PRO energy production. Therefore, the model net specific energy consumption (SE_{sys}) for the RO-PRO system can be expressed as:

$$SE_{sys} = \frac{SEC_{RO,tr}^{ERD} * Q_{p,RO} + SE_{PRO} * Q_{p,PRO}}{Q_{p,RO}} \tag{32}$$

where SE_{sys} has units of kWh per m^3 of freshwater permeate produced by the RO-PRO system. SE_{sys} can be evaluated over a range of RO recoveries and PRO dilutions (i.e., PRO permeate flowrates).

2.3 Model Input – Membrane Modules and Flow Conditions

2.3.1 RO Sub-System

The RO membrane characteristics were based on a Dow FilmTec (Midland, MI) SW30-4040 membrane with 99.4 percent NaCl rejection. The RO feed solution was based on seawater with a concentration of 3.5 percent NaCl and an osmotic pressure of 2879 kPa calculated using OLI Stream Analyzer 2.0. The RO pump and ERD efficiencies were selected as 80 and 95 percent, respectively, to be consistent with previous RO model predictions [39].

2.3.2 PRO Sub-System

The PRO membrane characteristics were based on the Hydration Technology Innovations (HTI) (Albany, OR) CTA membrane. The water permeability coefficient, salt permeability coefficient, and structural parameter used were 1.87E-9 (m/s)/kPa, 1.11E-7 m/s, and 6.87E-4 m, respectively[47]. The membrane module size (8 in diameter and 40 in length) was based on an HTI 8040 PRO spiral wound membrane module with a membrane area of 15 m^2. This size module is standard for FO and RO applications and the pressure vessel is commercially available. A channel height of 0.38 mm, a spacer porosity of 0.65, and a spacer specific surface area of 19.5 mm^{-1} were selected based on previously reported values for RO spiral wound elements in the literature[51] because values are not currently available for the HTI 8040 PRO module.

When evaluating the ability of PRO to dilute RO brine back to seawater concentration (using 5 to 70 percent PRO dilution), the PRO draw solution concentration ranged from 37 to 117 g/L NaCl, which corresponds to 5 to 70 percent RO recovery. For other RO-PRO system evaluations, the brine concentration ranged from 50 to 87.5 g/L NaCl for 30 to 60 percent RO recovery. The PRO feed solution salinity was zero in order to maximize the osmotic pressure difference across the membrane, and in turn, maximize the driving force. The PRO hydraulic pressure difference was incrementally increased until a maximum power density was accomplished. By maximizing the power density, the SE_{PRO} was also maximized.

A PRO feed flowrate of 18 m^3/d was selected as it falls within the manufacturer suggested range for an 8040 module[52]. A PRO draw solution flowrate of 117 m^3/d was selected as it also falls within the manufacturer suggested range [52] as well as results in a draw solution velocity of 0.24 m/s and corresponds to a *Re* of approximately 130, which falls in the typical range ($50 < Re < 200$) for spiral wound modules [53, 54]. To produce the constant draw solution flowrate required, RO feed flowrates of 167, 195, 234, and 293 m^3/d were used for RO recoveries of 30, 40, 50, and 60 percent, respectively. To increase the PRO sub-system contribution, membranes module were added only in parallel.

2.4 Model Results

2.4.1 RO Model Results

In figure 6a, the $SE_{RO,tr}$ (Eq. 11) of a model RO sub-system with and without an ERD at the thermodynamic restriction is given as a function of recovery. For the RO sub-system without an ERD, the minimum specific energy consumption is 3.82 kWh/m^3 at 50 percent recovery. For the RO sub-system with an ERD (optimized RO), the minimum specific energy consumption is 1.45 kWh/m^3 at 13 percent recovery; at 50 percent recovery, the specific energy consumption is 2.00 kWh/m^3. Thus, at 50 percent recovery, the ERD reduces RO specific energy consumption by almost 50 percent; this was expected based on results of previous

studies [55]. Compared to the theoretical SE_{RO} consumption (figure 3b), the model results (with ERD) require approximately double the specific energy of the ideal case. This is because the model operates as an irreversible thermodynamic process and assumes a finite process size.

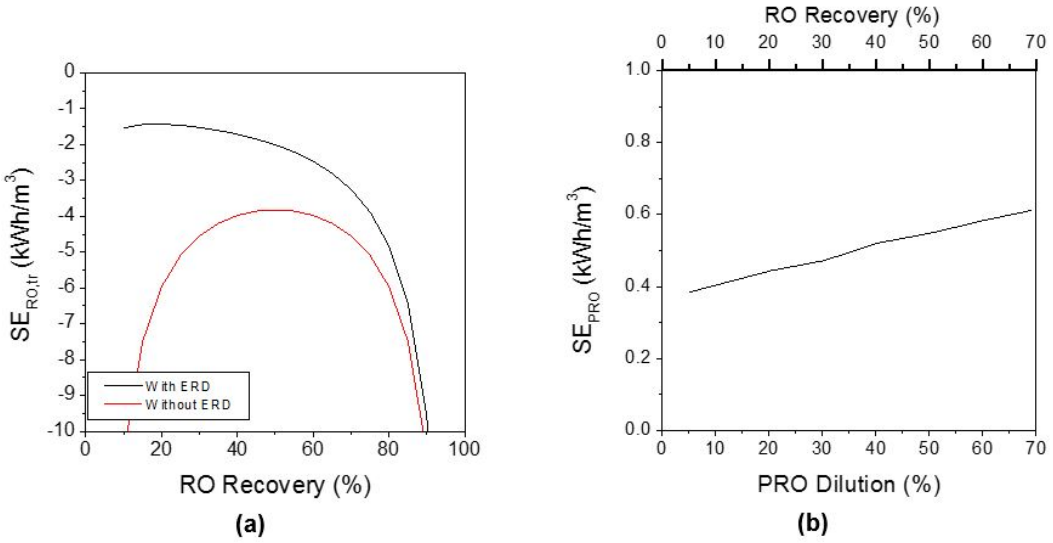

Figure 6.—(a) RO specific energy consumption at the thermodynamic restriction (SEC_{tr}) modeled as a function of recovery with and without an energy recovery device (ERD). Pump efficiency, membrane salt rejection, and ERD efficiency were taken as 80%, 99.4%, and 95%, respectively. (b) PRO specific energy production (SE_{PRO}) modeled as a function of dilution (%) for a CTA membrane with optimal PRO hydraulic pressure (from approximately 1400 to 2200 kPa) and a feed flowrate of 18 m^3/d. Exiting draw solution concentration ($C_{ds,ex}$) is 35 g/L NaCl.

2.4.2 PRO Model Results

In figure 6b, the SE_{PRO} production (Eq. (31)) of the PRO sub-system when diluting RO brine back to seawater concentration is given as a function of RO recovery and PRO dilution. As RO recovery increases, the entering draw solution concentration increases and thus, PRO dilution increases. The minimum SE_{PRO} production is approximately 0.4 kWh/m^3. The SE_{PRO} production increases with increasing RO recovery and the maximum SE_{PRO} production is approximately 0.6 kWh/m^3 at 70 percent dilution. Compared to the theoretical SE_{PRO} production (figure 3d), the model case produces approximately half the specific energy of the ideal case. This is because the PRO model also operates as an irreversible thermodynamic process and assumes a finite process size. The differences between the ideal and model results, together with the effects of membrane characteristics and concentration polarization effects, are discussed in the next section for the complete RO-PRO system.

2.4.3 RO-PRO System Model Results

Figure 7 is a comparison of the *SE* values from the ideal case (figure 4) with the model RO-PRO results. For both the ideal case and the model results, the maximum SE_{sys} consumption point for each RO recovery is the point at which there is no PRO sub-system contribution (dilution = 0). As PRO dilution increases (more PRO membranes being added), the SE_{sys} consumption decreases due to increased PRO dilution. Also, for both, the higher the RO recovery, the higher the maximum SE_{RO} consumption. However, for each recovery, the maximum SE_{sys} consumption for the model results is approximately double that for the ideal case. As expected, the slopes of the lines are much higher for the ideal case than for the model results. This is because the ideal SE_{PRO} production is approximately twice the model SE_{PRO} production. Because of the higher starting model SE_{sys} consumption and because of the lower rate at which the model SE_{sys} consumption decreases, the model RO-PRO system cannot reach energetic neutrality; energy is required to produce water.

The model was also used to predict the maximum PRO dilution and minimum SE_{sys} consumption for the four RO recoveries. Because of the finite amount of draw solution, there is a point where adding PRO membranes no longer increases dilution or decreases the SE_{sys} consumption because the PRO draw solution has reached maximum dilution. Maximum dilutions occur at 48, 55, 72, and 73 percent for 30, 40, 50, and 60 percent recoveries, respectively. The minimum SE_{sys} values corresponding to these maximum dilutions are 0.58, 0.90, 1.23, and 1.76 kWh/m^3, respectively.

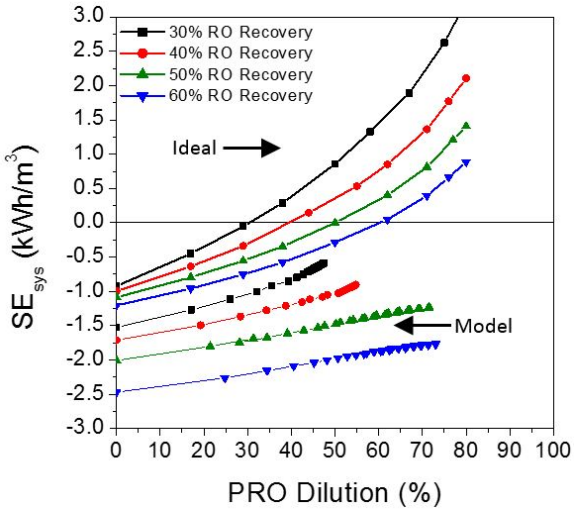

Figure 7.—Comparison of net model results (with the ideal and model cases) RO-PRO specific energy as a function of PRO dilution for several RO recoveries.

A sensitivity analysis was conducted to determine the effects of PRO membrane characteristics on the RO-PRO system energy requirements. Sixty-four virtual membranes were created with varying combinations of water permeability, salt

permeability, and structural parameter. In table 1, the first row (A1, B1, S1) represents the original CTA membrane characteristics. The second row (A2, B2, S2) represents a virtual membrane with an order of magnitude higher water permeability, an order of magnitude lower salt permeability, and an order of magnitude lower structural parameter compared to the CTA membrane. The third row (A3, B3, S3) represents a virtual membrane with two orders of magnitude higher water permeability, two orders of magnitude lower salt permeability, and two orders of magnitude lower structural parameter compared to the CTA membrane. The fourth row (A4, B4, S4) represents a virtual membrane with an order of magnitude lower water permeability, an order of magnitude higher salt permeability, and an order of magnitude higher structural parameter compared to the CTA membrane. It would be expected that row three represents the best characteristic combination followed by rows two, one, and four.

Table 1.—Values of A, B, and S Used in the Sensitivity Analysis Where Row One Is the CTA Membrane

	A (m/s)/kPa	B (m/s)	S (m)
1	1.87E-09	1.11E-07	6.87E-04
2	1.87E-08	1.11E-08	6.87E-05
3	1.87E-07	1.11E-09	6.87E-06
4	1.87E-10	1.11E-06	6.87E-03

The 64 virtual membranes were analyzed using the RO-PRO model assuming 50 percent RO recovery. The sensitivity analysis results for the SE_{sys} consumption of the RO-PRO system are shown in figure 8; salt permeability is presented on the x-axis, water permeability is presented on the y-axis, structural parameter is presented on the z-axis, and SE_{sys} consumption is indicated by color gradient. For a consistent comparison, all virtual membrane SE_{sys} consumption values are for 30 membranes arranged in parallel. A configuration of 30 membranes in parallel was chosen to accomplish a significant amount of PRO permeate and still observe a significant decrease in specific energy requirement. As the water permeability increases for each salt permeability and structural parameter, the SE_{sys} consumption decreases because increased water permeability allows for higher water flux through the membrane. Also, as the salt permeability decreases, the SE_{sys} consumption decreases because decreased reverse salt flux and decreased concentration polarization allows for maximum draw solution utilization. In other words, the concentration gradient is not decreased by reverse salt flux and concentration polarization. Lastly, as the structural parameter decreases, the SE_{sys} consumption decreases because concentration polarization effects are minimized and hence water flux increases. There are also four combinations that did not work according to the model; these were not included in figure 10. These four combinations consisted of both B4 and S4. Membranes with combined high salt permeability and a large structural parameter result in instantaneous loss of driving force due to accelerated reverse salt flux by severe internal concentration polarization.

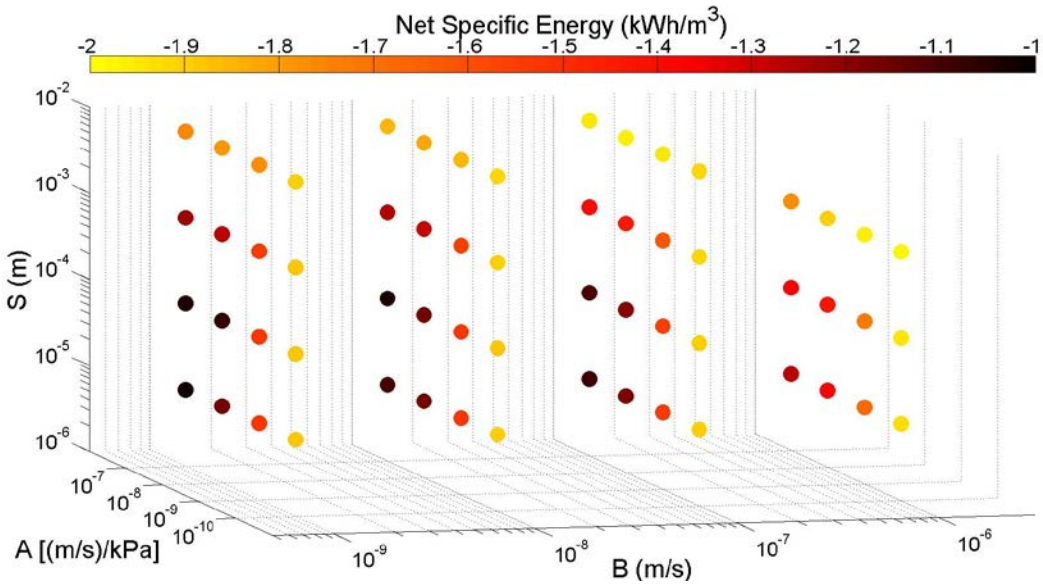

Figure 8.—RO-PRO net specific energy sensitivity analysis results for 64 virtual membranes analyzed in a parallel configuration (30 total membrane modules) using the RO-PRO model with 50% RO recovery flow conditions.

Data from the nine best performing membrane combinations together with the original CTA membrane (A1, B1, S1) were extracted from figure 8 and are presented in table 2. These are the virtual membranes that enabled the RO-PRO system to approach its minimum SE_{sys} consumption of approximately 1.0 kWh/m^3. As expected, the virtual PRO membranes that minimize SE_{sys} consumption have high water permeability, low salt permeability, and small structural parameter. Consequently, the best performing membrane in terms of low SE_{sys} consumption, high permeate flowrate, and high power density is the membrane with the greatest improvement in characteristics: A3, B3, S3. Besides minimizing SE_{sys} consumption, a high power density is desirable in the RO-PRO system because it reduces the required membrane area. The SE_{sys} consumptions and power densities are only marginally different for the nine virtual membranes. However, when compared to the CTA membrane (A1, B1, S1), the virtual membranes have an SE_{sys} consumption approximately 35 percent lower and a power density more than two times higher. It is also worth noting that utilizing the new model for full-scale PRO applications results in a power density reduction of approximately 70 percent compared to models for bench-scale PRO applications [47]. Furthermore, from table 2 it can be seen that power density does not exceed approximately 10 W/m^2, regardless of membrane characteristics. This power density cap should be considered when emphasizing the need for new and improved PRO membranes.

Figure 9 summarizes the SE_{sys} consumption with increasing hydraulic pressure for (a) increasing water permeability, (b) decreasing salt permeability, (c) decreasing structural parameter, and (d) combined improvement of all three characteristics. For each membrane characteristic combination, the SE_{sys} consumption reaches a

Table 2.—Best Performing Combinations from Sensitivity Analysis

Combination	SE_{sys} (kWh/m^3)	Permeate Flowrate (m^3/d)	Membranes in Parallel	Power Density (W/m^2)
A1, B1, S1	-1.62	68	30	4.21
A2, B2, S3	-1.16	223	30	9.10
A2, B3, S2	-1.07	230	30	10.13
A2, B3, S3	-1.16	223	30	9.13
A3, B1, S2	-1.10	231	30	9.73
A3, B1, S3	-1.09	234	30	9.93
A3, B2, S2	-1.04	313	30	10.43
A3, B2, S3	-1.10	231	30	9.73
A3, B3, S2	-1.03	315	30	10.48
A3, B3, S3	-1.02	347	30	10.62

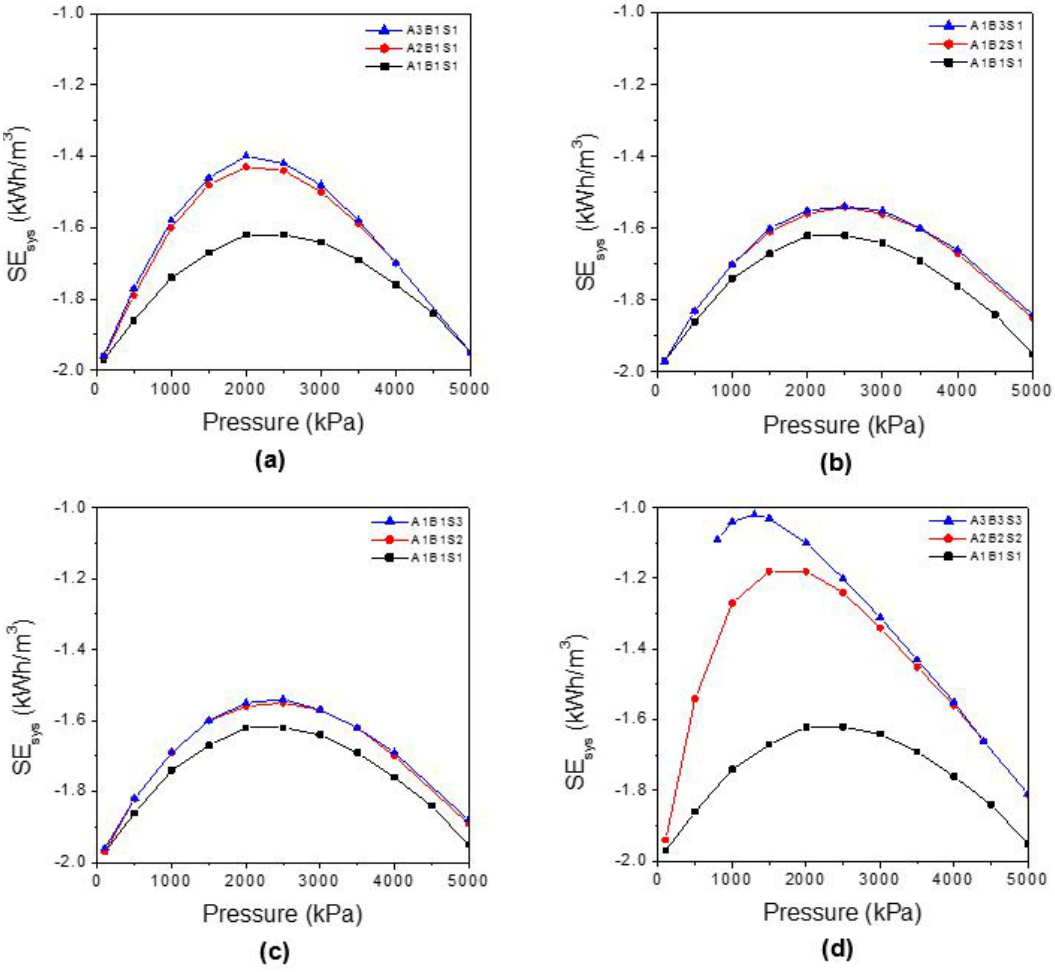

Figure 9.—*SE$_{sys}$* with increasing pressure for (a) increasing water permeability, (b) decreasing salt permeability, (c) decreasing structural parameter, and (d) improvement of all three characteristics using 50% RO recovery flow conditions.

minimum value at a unique optimal hydraulic pressure. When taken individually, increasing water permeability (figure 9a), decreasing salt permeability (figure 9b), and decreasing structural parameter (figure 9c) do not result in significant decreases in SE_{sys} consumption compared to the combined improvement combinations of the three characteristics (figure 9d). While the optimal hydraulic pressure for increasing water permeability (figure 9a) decreases from approximately 2,500 kPa to approximately 2,000 kPa, the optimal hydraulic pressures for decreasing salt permeability (figure 9b) and structural parameter (figure 9c) alone do not significantly change. However, when the three characteristics are simultaneously improved (figure 9d), the optimal hydraulic pressure decreases to approximately 1,500 kPa. As water flux increases and salt permeability (or reverse salt flux) decreases, the effective osmotic pressure decreases according to Eq. (13). Because the optimal hydraulic pressure difference for PRO is half the effective osmotic pressure, the optimal hydraulic pressure also decreases. Lower hydraulic pressure is an added benefit because typically, the fabrication of membranes and system components for lower pressures is more economical.

Based on the sensitivity analysis, the manufacture of next generation membranes should focus on all membrane characteristics but should prioritize efforts on improving water permeability because this will increase the power density and decrease the specific energy requirement the most. Newer concepts for improving membrane performance include use of aquaporins (water-selective proteins) and nano-materials [56, 57]. Aquaporins have shown an improvement in water permeability by one order of magnitude compared to CTA RO membranes [56]. Nano-materials also offer high water permeability [57]. Aquaporins or nano-materials could be similar to the virtual membrane (A3, B1, S2) (one of the top-performing membranes in table 2) where the water and the structural parameter are improved but the salt permeability is similar to CTA membranes. However, membranes from these materials are still in the experimental stage and other aspects (e.g., cost and membrane life) need to be considered before recommending use on a large scale.

3. EXPERIMENTAL

3.1 Membrane Modules, Devices, and Testing Conditions

3.1.1 RO Sub-system

Three spiral wound RO membrane modules (SW30-2540, Dow FilmTec, Midland, MI) were installed into high pressure vessels in the small-scale pilot. Each module had an active membrane surface area of 2.8 m^2. The membrane modules were arranged in series so that the concentrated brine leaving the one module was the feed solution for the subsequent module. According to

manufacturer recommendations, feed pressure and flowrate were gradually increased over a 30- to 60-second time period in order to avoid possible membrane damage. In addition, after initial wetting occurred, the elements were kept moist at all times to preserve the membranes. The manufacturer rated salt rejection for SW30-2540 modules is 99.4 percent.

3.1.2 PRO Sub-system

One 4040 spiral wound PRO membrane module (Oasys Water, Boston, MA) with an active membrane surface area of approximately 4.18 m^2 was installed into a high pressure vessel in the small-scale pilot RO-PRO system. According to the manufacturer, the water permeability coefficient (A), salt permeability coefficient (B), and structural parameter (S) for the PRO membrane was 1.42E-8 (m/s)/kPa, 2.41E-8 m/s, and 3.10E-4 m, respectively. In the PRO membrane module, it was essential that the envelope was not over-pressurized and that the hydraulic pressure of the feed solution never exceeded the hydraulic pressure of the draw solution in order to avoid damage to the membrane. In addition, a freshwater flush was required after shutdown of the system so that water would not continue to transfer from the feed solution side to the draw solution side.

3.1.3 Pressure Exchanger (PX)

An XPR (aXle Positioned Rotor) PX from Isobaric Strategies, Inc. (Virginia Beach, VA) was used in the small-scale pilot RO-PRO system. This PX works via a displacement method. A high-pressure stream enters the PX and turns a rotor that pressurizes a low pressure stream on the other side. In the RO-PRO system, the high pressure draw solution exiting the PRO sub-system was used to pressurize the low pressure seawater stream entering the RO subsystem. In this way, the RO feed solution was pressurized before the high pressure pump in order to decrease the work done by the pump.

The PX efficiency is dependent on the matched flowrates entering and exiting the device. If the flowrates are unmatched, leaking occurs within the device until all flows are balanced. Therefore, in addition to monitoring the pressures entering and exiting the PX, the flowrates were also monitored to determine the internal circulation flow within the PX. The ports of the PX were monitored with dial pressure gauges, low pressure transducers, acrylic flow meters (Cole-Palmer, Vernon Hills, IL), and high pressure flow sensors (GF Signet, El Monte, CA). Similarly, the high pressure inlet and outlet of the PX were monitored with high pressure transducers (Cole-Parmer, Vernon Hills, IL). In this way, the pressure efficiency (η_{Press}) can be calculated as:

$$\eta_{Press} = \frac{P_2 - P_1}{P_3 - P_4} \tag{33}$$

where the subscripts *1*, *2*, *3*, and *4* indicate the low pressure entering port, high pressure exiting port, high pressure entering port, and low pressure exiting port, respectively. The efficiency of the PX can also be calculated based on the concentration (η_{Conc}):

$$\eta_{Conc} = \frac{C_3 - C_2}{C_3 - C_1} \tag{34}$$

If the PX leaks, then the high pressure outlet will have a different concentration from the low pressure inlet. It is important to establish the two efficiencies of the PX in order to recover the most energy without increasing the concentration in the feed solution with brine solution mixing.

3.1.4 Testing Conditions

Testing was conducted at the Reclamation's *Brackish Groundwater National Desalination Research Facility* in Alamogordo, NM, and the University of Nevada, Reno Laboratories (figure 10). Testing was separated into three categories: RO alone (figure 11a), RO-PX (figure 11b), and RO-PRO (figure 11c). All three setups had the same flowrate entering the system (5.0 LPM) and were tested with freshwater recoveries of 20 and 30 percent. Simulated seawater was used as the RO feed solution for all configurations, and in the case of RO-PRO, filtered (1 µm) municipal tap water was used for the PRO feed solution. Using tap water instead of wastewater avoids the fouling issues that have afflicted previous systems so that the maximum potential of the RO–PRO system can be assessed. The concentration of the simulated seawater entering the system was approximately 35 to 37 g/L with the concentration entering the RO sub-system ranging between 33 and 35 g/L depending on the configuration. Operating hydraulic pressures ranged between 500 and 700 psi in order to accomplish the desired freshwater recoveries. The pressure was established using a needle valve.

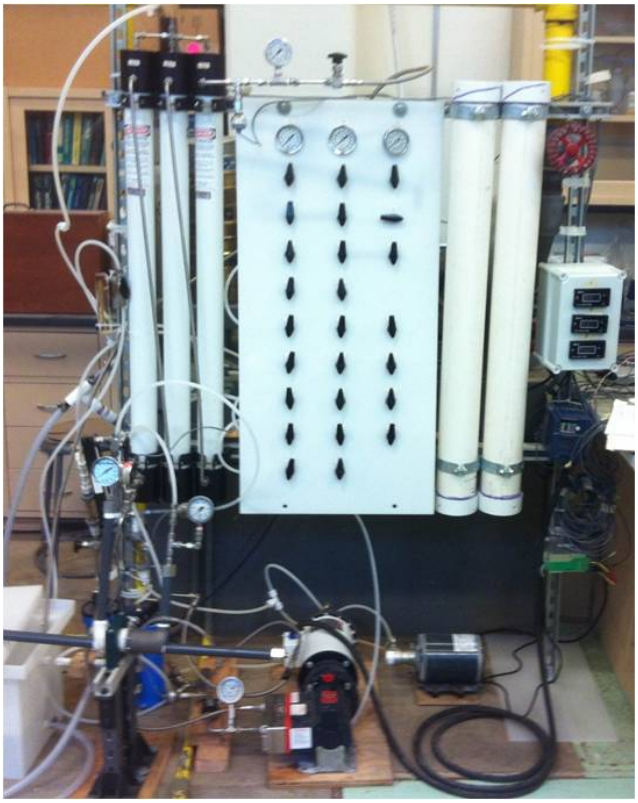

Figure 10.—RO-PRO pilot system in the University of Nevada, Reno laboratory.

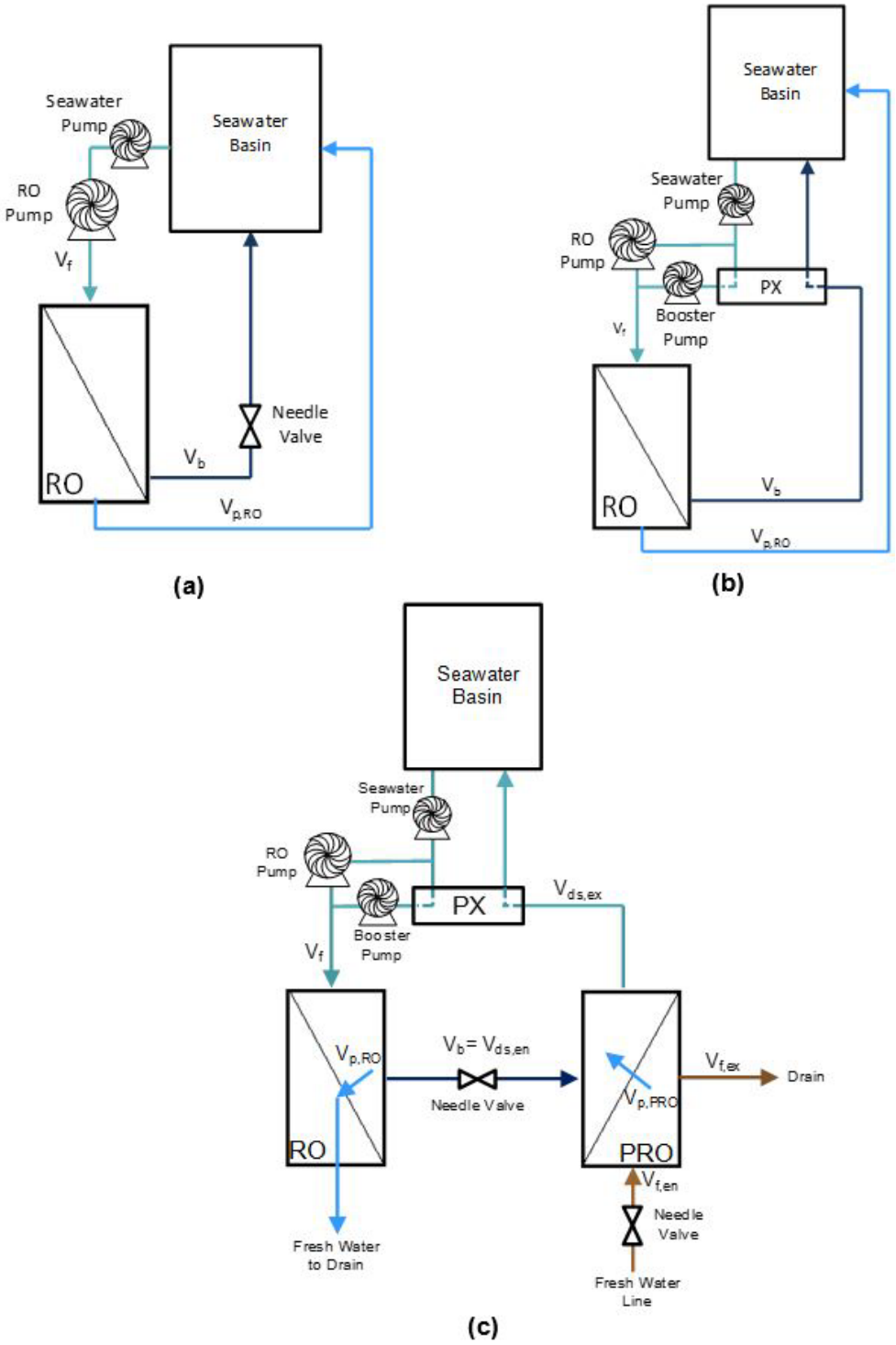

Figure 11.—(a) RO alone configuration, (b) RO-PX configuration, and (c) RO-PRO configuration where V_f, V_b, and $V_{p,RO}$ are the RO feed, brine, and permeate volumes, respectively and $V_{ds,en}$, $V_{ds,ex}$, $V_{f,en}$,$V_{f,ex}$, and $V_{p,PRO}$ are the PRO draw solution entering, draw solution exiting, feed solution entering, feed solution exiting, and permeate volumes, respectively.

This valve decreased the pressure of the brine stream leaving the RO module to the pre-determined design pressure of the PRO module. The energy from this pressure drop is therefore lost to the environment as heat. The PRO feed solution pressure ranged from 15 to 35 psi. This was well below the draw solution pressure range of 100 to 250 psi so there was no chance the PRO membrane envelope could be over-pressurized and damage the membrane. Each configuration also required a different number of Hydra-Cell (Wanner Engineering, Inc., Minneapolis, MN) diaphragm variable-speed pumps. The RO alone scenario required two pumps while the RO-PX and RO-PRO required three pumps (seawater pump, RO pump, and booster pump). To calculate efficiency of the pump system, the required power (flow rate times pressure difference across the pump) is divided by the observed power consumption read from either the motor drive or the plug-in Kill-A-Watt meter (P3 International, New York, NY):

$$\eta_{pump\ system} = \frac{Required\ Power}{Observed\ Power} \tag{35}$$

3.2 Experimental Results

3.2.1 RO Experimental Results

Testing the pilot RO sub-system alone established a baseline SE_{RO} for the RO-PRO pilot system. For 20 and 30 percent recovery, the SE_{RO} is 12.83 and 9.67 kWh/m^3 where SE_{RO} is calculated using the power reading from the motor drive divided by the RO permeate flowrate. As expected, the higher recovery has a lower SE_{RO}. Optimally, a full scale RO sub-system should operate at a recovery of approximately 50 percent in order to accomplish the lowest SE_{RO} as seen in previous theory and modeling. However, due to the small size of the pilot RO sub-system, reaching 50 percent recovery was not possible.

3.2.2 RO-PX Experimental Results

A PX was then added to the RO sub-system in order to recover the energy from the high pressure brine solution. Note that this RO-PX configuration is not the same as the optimized RO used in Section 2.5 as the RO sub-system is not operated at the thermodynamic restriction. This is the traditional setup of a PX where the high pressure of the brine solution is transferred by the PX into the RO feed solution (figure 11b). The recovery, specific energy for RO-PX ($SE_{RO\text{-}PX}$), and PX and pump system efficiencies are given in table 3. Total power increases from 20 percent recovery to 30 percent recovery due to the increase in pressure to accomplish the higher recovery, but the permeate flowrate also increases with increasing recovery; the result is a lower $SE_{RO\text{-}PX}$ for the 30 percent recovery. Compared to the RO alone configuration, the $SE_{RO\text{-}PX}$ is noticeably higher. In terms of exchanging pressure (figure 12), the PX has high efficiency rates (i.e., above 90 percent). In terms of exchanging concentration, the efficiency differs for 20 and 30 percent recoveries. This is partially due to difficulty in obtaining

samples from the high pressure streams. Stainless steel ports consisting of a ball valve and tee were setup to gather water samples in the high pressure sections of the RO-PRO system. However, opening the valves significantly lowered the pressure of the section, and samples were taken in short bursts of opening the valves. This was to reduce the possibility of effecting the samples due to a sudden reduction in system pressure. Unavoidably, there is error in the concentration of these areas because the pressure declined despite efforts to quickly take water samples. A concentration efficiency higher than 100 percent mathematically means that salt concentration transfers from the entering seawater stream into the system exiting stream. Because of the unknown numerical error in taking high pressure samples, this is not true especially since the system exiting stream has a higher concentration than the entering system stream. From the table, it can be observed that the pump systems are operating with relatively low efficiency (4-40 percent). This is the likely reason for the increased energy requirement between the RO alone and RO-PX configurations. The low pump efficiencies will be discussed in more detail in the next section.

Table 3.—Kill-A-Watt Results from RO-PX Using Two Desired Freshwater Recoveries

		20% Recovery	30% Recovery
$SE_{RO\text{-}PX}$	kWh/m^3	13.50	11.28
PX Pressure Efficiency	%	93	95
PX Concentration Efficiency	%	112	77
Seawater Pump Efficiency	%	10	9
Booster Pump Efficiency	%	4	4
RO Pump Efficiency	%	34	40

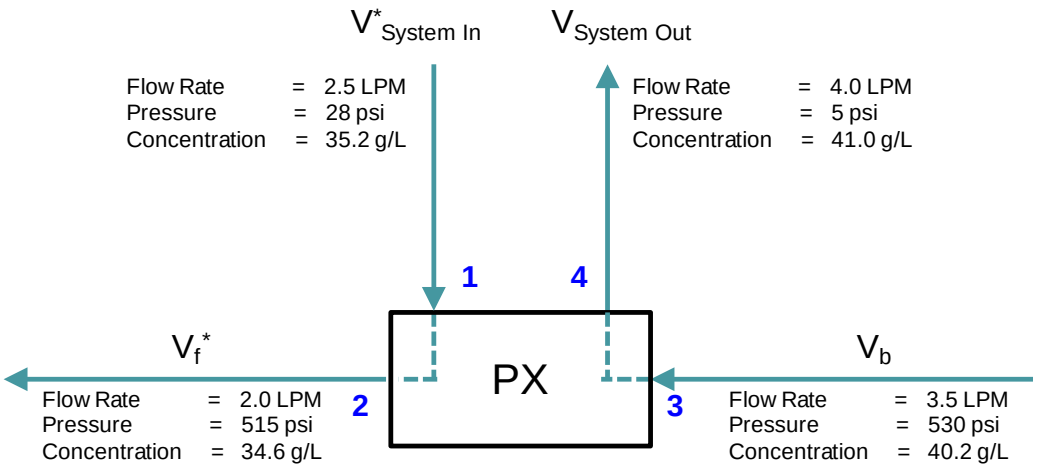

Figure 12.—Flowrates, pressures, and concentrations entering and exiting the PX for 20% RO recovery where (1) is the entering low pressure port or fraction of the system entering stream ($V^*_{System\ In}$), (2) is the exiting high pressure port or fraction of the RO feed (V_f^*), (3) is the entering high pressure port or RO brine (V_b), and (4) is the exiting low pressure port or exit from the system.

3.2.3 RO-PRO System Experimental Results

The small-scale pilot RO-PRO system has a similar set-up to the RO-PX configuration only with the added PRO sub-system that uses the RO concentrated brine as a draw solution (figure 11c). The results of the RO-PRO pilot system are presented in table 4. During the RO-PRO experiments, the draw solution pressure was varied using the PX and RO pump. The draw solution pressure increases when the speed of the RO pump motor also increases. In this way, the pressure to the PRO is controlled in addition to the pressure entering the PX.

The operating conditions (specific flowrates, pressures, and concentrations) for the RO-PRO tests are provided in Appendix C. Average results for the four tests are shown in figure 13. As can be seen by the relatively large error bars, one challenge with the small-scale pilot RO-PRO system was inconsistency between tests. This is likely a result of wetting issues across the length of the membrane. Due to flowrate restrictions of the small-scale pilot RO-PRO system, the desired wetout conditions were not attainable. Again, the SE_{sys} has increased from the RO-PX configuration due to the low pump efficiencies, although the increase is not as large as the increase from the RO alone to the RO-PX configuration. The average experimental power densities for the small-scale pilot RO-PRO system ranged from 1.1 to 2.3 W/m^2. This is higher than that reported for the river-to-sea PRO pilot system in Korea (1.5 W/m^2) [58] and approaches the goal of 5 W/m^2 that would make PRO an economically feasible technology [59]. The design of the system was originally based on PRO membranes that existed in 2010. In the last three years, PRO membrane technology has improved (water and salt permeabilities have improved an order of magnitude each); the improved membranes increase system performance but also create an operational challenge for the small-scale pilot RO-PRO system that was designed for lower membrane performance. This is evident in the low pump system efficiencies presented in table 4. For this reason, it is desirable to replace the pump systems with ones that can accommodate higher flowrates and efficiencies. This would reduce overall RO-PRO energy consumption and improve overall system efficiency.

Table 4.—RO-PRO Pilot System Results with 20 and 30% Recoveries and Increasing Draw Solution Pressure

		20% Recovery				30% Recovery			
Operational PRO Draw Solution Pressure		**100 psi**	**150 psi**	**200 psi**	**250 psi**	**100 psi**	**150 psi**	**200 psi**	**250 psi**
PX Pressure Efficiency	%	35	64	75	81	48	69	78	82
Power Density	W/m^2	1.85	2.12	1.78	1.11	2.13	2.29	2.03	1.54
Seawater Pump Efficiency	%	15	15	14	14	14	13	12	12
Booster Pump Efficiency	%	48	46	43	40	52	50	49	46
RO Pump Efficiency	%	31	21	27	23	31	30	30	36
SE$_{sys}$	kWh/m^3	14.76	14.31	14.79	14.50	11.19	11.16	11.49	11.70

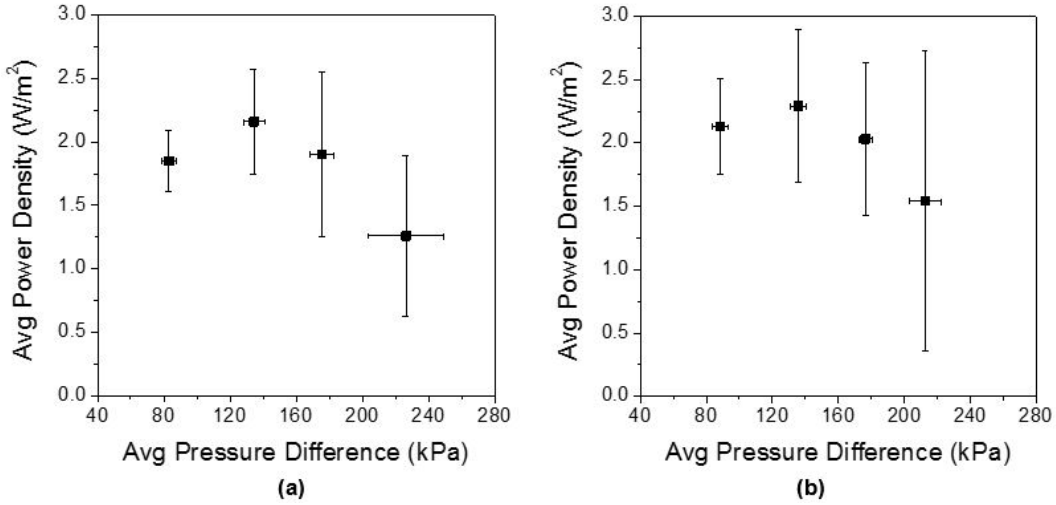

Figure 13.—Average power density with increasing hydraulic pressure difference for (a) 20% RO recovery and (b) 30% RO recovery.

3.2.4 PRO Alone

The PRO sub-system was also tested independent of the RO-PRO system to determine PRO sub-system performance (table 5). During RO-PRO testing, the exiting feed solution salt concentration increased as draw solution pressure increased, indicating that the salt permeability varied as operational conditions changed. Therefore, the salt and water permeability coefficients were calculated using the known entering and exiting concentrations, pressures, and flow rates from table 5.

Table 5.—Results for PRO Alone Test Using Seawater and Increasing Draw Solution Pressure

$PRO_{DS,en}$ Pressure (psi)	$PRO_{DS,en}$ Concentration (g/L)	$PRO_{DS,ex}$ Concentration (g/L)	$PRO_{F,en}$ Concentration (g/L)	$PRO_{F,ex}$ Concentration (g/L)	PRO Permeate Flow Rate (LPM)	$PRO_{F,en}$ Pressure (psi)
30	35.1	27.4	0.0	0.6	1.2	15
50	35.1	28.5	0.0	0.7	1.0	15
70	34.8	28.7	0.0	0.8	0.8	18
100	34.7	29.6	0.0	0.9	0.5	20
150	34.5	30.9	0.0	1.2	0.3	28
200	34.1	31.7	0.0	1.4	0.0	38
250	33.4	32.4	0.0	1.6	-0.2	58

The calculated salt permeability coefficient (figure 14a) increases with increasing draw solution pressure. In addition, the water permeability coefficient (figure 14b) decreases as draw solution pressure increases. These account for the decrease in PRO permeate flow rate along with the increase in exiting feed solution concentration as draw solution pressure increases. In theory, PRO membranes

have a peak power density at a specific hydraulic pressure difference (equal to approximately half the osmotic pressure difference). However, if the salt permeability increases and the water permeability decreases as the draw solution pressure increases, the peak power density decreases. This occurs because the power density is based on water flux and hydraulic pressure. The goal in manufacturing PRO membranes would therefore be to have a minimum salt permeability and maximum water permeability in order to accomplish the largest power density. In turn, this would decrease the specific energy consumption of the RO-PRO system because the PRO sub-system would transfer a larger pressure to the RO feed solution. From the figure, the PRO membrane requires fine-tuning in order to accomplish this goal.

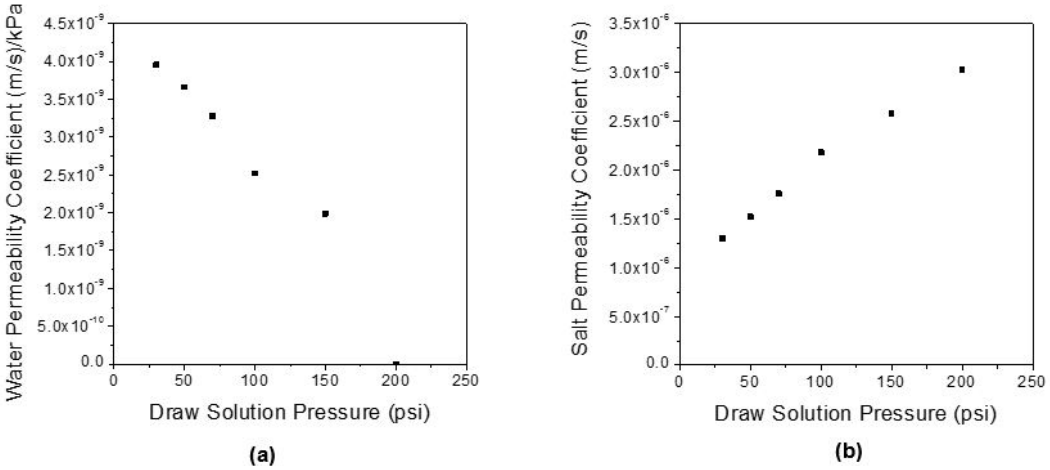

Figure 14.—Calculated PRO (a) water permeability coefficient and (b) salt permeability coefficient from experiments using variable draw solution pressure and constant seawater draw solution concentration (35 g/L NaCl)

3.2.5 RO-PRO Projected Results for High Efficiency Pump Systems

Specific energies of the configurations with pump systems that are projected to have efficiencies of 80 percent are shown in table 6. Specific energies were projected for the 150 psi draw solution pressure for 20 and 30 percent recovery. For all three configurations in table 6 there is a substantial reduction in the *SE projected* for the high efficiency pump systems compared to the *SE* for the actual pump systems.

The RO-PRO configuration can be improved even further. The third row in table 7 shows *SE* projections when a second PX is used to capture the wasted energy at the pressure drop between the RO brine stream and the PRO entering draw solution. Comparison of this data with the actual and projected high efficiency pump systems (rows 1 and 2) indicates that a second PX could reduce the *SE* by an additional 30 percent. The third row in table 7 is the most improved RO-PRO system and includes optimal power density in the system (approximately 5 W/m^2). The low flowrates of the pilot small-scale pilot RO-PRO system are only able to

achieve 2.3 W/m^2 power density. By increasing the flowrates and therefore power density, the RO-PRO system can potentially achieve an *SE* of 2.94 and 3.01 kWh/m^3 for 20 and 30 percent recovery, respectively. With the high efficiency pump system, the second PX, and optimal power density (third row in table 7) the RO-PRO system has approximately an 80 percent reduction in the projected *SE* compared to the actual *SE*.

Table 6.—Projected SE for All Configurations with Pump System Efficiencies of 80% and RO-PRO Using the Experimental Results for 150 psi for 20 and 30% Recovery

		20% Recovery	30% Recovery
Experimental RO Alone SE_{RO}	kWh/m^3	12.83	9.67
Projected RO Alone with High Efficiency Pump System	kWh/m^3	6.25	5.04
Experimental RO-PX $SE_{RO\text{-}PX}$	kWh/m^3	13.50	11.28
Projected RO-PX with High Efficiency Pump System	kWh/m^3	3.16	3.44
Experimental RO-PRO SE_{sys} ($PRO_{DS,en}$ Pressure=150 psi)	kWh/m^3	19.65	13.44
Projected RO-PRO with High Efficiency Pump System	kWh/m^3	6.23	5.27

Table 7.—Projected SE for All Configurations with Pump System Efficiencies of 80% for RO-PRO Using the Experimental Results for 150 psi for 20 and 30% Recovery

		20% Recovery	30% Recovery
Experimental RO-PRO SE_{sys} ($PRO_{DS,en}$ Pressure of 150 psi)	kWh/m^3	14.31	11.16
Projected RO-PRO with High Efficiency Pumps	kWh/m^3	6.23	5.27
Projected RO-PRO with High Efficiency Pumps, 2nd PX, and Optimal Power Density	kWh/m^3	2.94	3.01

While the second PX and increased power density reduce the RO-PRO SE_{sys}, the greatest projected reduction in SE_{sys} is achieved with high efficiency pump systems. It is also important to note that the RO system is not operated at the thermodynamic limit as discussed in the theory section (Section 2.2.1). From figure 6a the $SE_{RO,tr}$ for 20 percent RO recovery with and without an ERD is 1.43 and 5.97 kWh/m^3, respectively, and the $SE_{RO,tr}$ for 30 percent RO recovery with and without an ERD is 1.52 and 4.55 kWh/m^3, respectively. Operating the RO system at the thermodynamic restriction would further reduce the specific energy consumption of the RO-PRO system. According to the model, if the RO-PRO pilot system is operated at 50 percent RO recovery, the SE_{sys} would be approximately 1.72 kWh/m^3. This is a significant reduction from the optimized SE_{sys} for 20 percent and 30 percent in table 7. Therefore, a full-scale RO-PRO system should operate with RO at approximately 50 percent recovery and with 80 percent efficiency pump systems in order to realize energy savings from the system.

3.2.6 RO-PRO System Upgrades Proposed for Future Gen-2 RO-PRO System

As stated earlier, there are multiple aspects of the Gen-1 system that can be improved to decrease overall system energy consumption. The most important is scaling up the pumps to accommodate the significant performance improvements that PRO membranes have seen in the past 3 years. In the Gen-1 system, high enough flow rates could not be achieved due to the RO subsystem and pumping constraints. A Gen-2 RO-PRO system would be improved by adding a second PX to capture the wasted energy at the pressure drop between the RO brine and PRO entering draw solution. Because of the success in demonstrating the exchange of pressure between PRO and RO in the Gen-1 system, a second PX is expected to be successful in ensuring all "waste" energy is recovered from RO. Furthermore (data not shown), by operating the RO sub-system near 50 percent recovery, further energy reductions can be accomplished [39, 60]. The Gen-1 RO sub-system could not achieve 50 percent recovery due to its small size. The design of a larger-size pilot system would enable the use of industry-standard energy efficient pumps and PXs.

3.2.7 Model and Experimental Comparison

Using the values for flowrate, pressure, and concentration determined from the RO-PRO testing, the model results can be compared to the experimental results to test the validity of the model (table 8). The difference between the experimental power density and model power density is not consistent for each draw solution pressure. There are a couple possible reasons why the experimental and model results vary from one another; the first is that the PRO was not experimentally operated at its optimal power density. Therefore, the conditions within the PRO membrane were not ideal to compare to the model and unexpected inefficiencies within the membrane module were present that are not accounted for in the model. The second is that the characteristics regarding the spacer for the PRO membrane module were not available and were therefore assumed in the model.

Table 8.—Experimental and model power densities with increasing PRO draw solution pressure

Recovery (%)	PRO Draw Solution Pressure (psi)	Experimental Power Density (W/m^2)	Model Power Density (W/m^2)	% Difference
30	100	2.13	2.49	14
30	150	2.29	3.51	35
30	200	2.13	3.23	34
30	250	1.54	3.87	60

4. CONCLUSIONS

During this investigation, the specific energy consumption of a RO-PRO system was modeled using RO conditions at the thermodynamic restriction and a novel module-based PRO model. Using a well-characterized CTA membrane, the minimum net specific energy consumption of the modeled system was 1.2 kWh/m^3 for 50 percent RO recovery. Considering an RO specific energy consumption of 2.0 kWh/m^3, the RO-PRO system can theoretically achieve 40 percent energy reduction.

A sensitivity analysis was performed to determine the effects of the membrane characteristics (A, B, and S) on the specific energy production of the PRO process in the RO-PRO system. The sensitivity analysis showed that the minimum system specific energy consumption using virtual membranes was approximately 1.0 kWh/m^3 of RO permeate at 50 percent RO recovery and that a maximum power density of approximately 10 W/m^2 could be achieved. Based on the sensitivity analysis, manufacturing of next generation membranes should focus on all membrane characteristics but should prioritize efforts on improving water permeability.

In addition, the model was tested by comparing the experimental results to those generated by the model using the same flowrates, pressures, and concentrations. The experimental results did not show the energy savings expected by the model. This was attributed to the inefficiencies of the system due to the need to scale up to accommodate the significant performance improvements that PRO membranes have seen in the past 3 years, unrecovered pressure drops, and operating PRO at a lower flowrate than recommended by the manufacturer to reach optimal power density. By scaling up the RO-PRO system and replacing the pump systems with more appropriate and efficient devices, the RO-PRO system was projected to see a considerable decrease in energy consumption.

The average experimental power densities for the RO-PRO system ranged from 1.1 to 2.3 W/m^2. This is higher than previous river-to-sea PRO pilot systems (1.5 W/m^2) and approaches the goal of 5 W/m^2 that would make PRO an economically feasible technology. In addition, this is the first known system to utilize energy from a volume of water transferred from atmospheric pressure to elevated pressure across a semi-permeable membrane to pre-pressurize RO feed water.

The RO-PRO system would also be competitive with leading renewable technologies including solar and wind power. The feasibility of PRO as a sustainable energy source can be evaluated by considering the coupling of the Ashkelon desalination facility in Israel with either PRO, solar, or wind power. Ashkelon covers approximately 25 acres and uses approximately 56 MW of power including ERDs [42]. A comparable PRO facility of the same size (25 acres) could theoretically produce approximately 14 MW and reduce

Ashkelon's power consumption to 42 MW (25 percent reduction). If Ashkelon were instead coupled with a solar farm, the solar farm would require approximately 100 acres for the same power reduction as a 25 acre PRO facility [61]. Similarly, if Ashkelon were coupled with a wind farm, the wind farm would require approximately 1110 acres for the same power reduction [62]. Even though an entire PRO facility would have to be built next to a desalination facility, the estimated land use is 25 percent of the required area for a similar solar farm and 3 percent of the required area for a similar wind farm. While there are many improvements still to be made in manufacturing PRO membranes and increasing efficiency of the RO-PRO system, it is a feasible technology that could greatly decrease desalination energy consumption and therefore provide affordable, fresh drinking water to water scarce areas of the world.

REFERENCES

[1] R. J. Aaberg. 2003. Osmotic Power: A New and Powerful Renewable Energy Source? *Refocus,* vol. 4, pp. 48-50.

[2] J. E. Hakes. 2000. The 25th Anniversary of the 1973 Oil Embargo. http://www.eia.doe.gov/emeu/25opec/anniversary.html

[3] R. S. Norman. 1974. Water Salination: A Source of Energy. *Science,* vol. 186, pp. 350-352.

[4] S. Loeb, F. V. Hessen, and D. Shahaf. 1976. Production of Energy from Concentrated Brines by Pressure-Retarded Osmosis: II. Experimental Results and Projected Energy Costs. *Journal of Membrane Science,* vol. 1, pp. 249-269.

[5] R. E. Pattle. 1954. Production of Electric Power by Mixing Fresh and Salt Water in the Hydroelectric Pile. *Nature,* vol. 174, p. 660.

[6] S. Loeb and R. S. Norman. 1975. Osmotic power plants. *Science,* vol. 189, pp. 654-655.

[7] G. D. Mehta and S. Loeb. 1978. Internal Polarization in the Porous Substructure of a Semipermeable Membrane under Pressure-Retarded Osmosis. *Journal of Membrane Science,* vol. 4, pp. 261-265.

[8] S. Loeb and G. D. Mehta. 1979. A Two Coefficient Water Transport Equation for Pressure-Retarded Osmosis. *Journal of Membrane Science,* vol. 4, pp. 351-362.

[9] H. H. Jellinek and H. Masuda. 1981. Osmo-power: Theory and Performance of an Osmo-Power Pilot Plant. *Ocean Engineering,* vol. 8, pp. 103-128,

[10] K. L. Lee, R. W. Baker, and H. K. Lonsdale. 1981. Membrane for Power Generation by Pressure Retarded Osmosis. *Journal of Membrane Science,* vol. 8, pp. 141-171.

[11] J. R. McCutcheon and M. Elimelech. 2008. Influence of Membrane Support Layer Hydrophobicity on Water Flux In Osmotically Driven Membrane Processes. *Journal of Membrane Science,* vol. 318, pp. 458-466.

[12] Y. Xu, X. Peng, C. Y. Tang, Q. S. Fu, and S. Nie. 2010. Effect of Draw Solution Concentration and Operating Conditions on Forward Osmosis and Pressure Retarded Osmosis Performance in a spiral Wound Module. *Journal of Membrane Science,* vol. 348, pp. 298-309.

[13] J. Su, S. Zhang, H. Chen, H. Chen, Y. C. Jean, and T. S. Chung. 2010. Effects of Annealing on the Microstructure and Performance of Cellulose Acetate Membranes for Pressure-Retarded Osmosis Processes. *Journal of Membrane Science*, vol. 364, pp. 344-353.

[14] H. Enomoto, M. Fujitsuka, T. Hasegawa, M. Kuwada, A. Tanioka, and M. Minagawa. 2010. A Feasibility Study of Pressure-Retarded Osmosis Power Generation System Based on Measuring Permeation Volume Using Reverse Osmosis Membrane. *Electrical Engineering in Japan*, vol. 173.

[15] N. Y. Yip and M. Elimelech. 2011. Performance Limiting Effects in Power Generation from Salinity Gradients by Pressure Retarded Osmosis. *Environmental Science & Technology*, vol. 45, pp. 10273-10282.

[16] J. T. Arena, B. McCloskey, B. D. Freeman, and J. R. McCutcheon. 2011. Surface Modification of Thin Film Composite Membrane Support Layers with Polydopamine: Enabling Use of Reverse Osmosis Membranes in Pressure Retarded Osmosis," *Journal of Membrane Science*, vol. 375, pp. 55-62,

[17] E. Sivertsen, T. Holt, W. Thelin, and G. Brekke. 2012. Pressure Retarded Osmosis Efficiency For Different Hollow Fibre Membrane Module Flow Configurations. *Desalination*, vol. 312, pp. 107-123.

[18] Y. C. Kim and M. Elimelech. 2012. Adverse Impact of Feed Channel Spacers on Performance of Pressure Retarded Osmosis. *Environmental Science & Technology*, vol. 46, pp. 4673-4681.

[19] I. L. Alsvik, K. R. Zodrow, M. Elimelech, and M. B. Hagg. 2013. Polyamide Formation on a Cellulose Triacetate Support for Osmotic Membranes: Effect of Linking Molecules on Membrane Performance. *Desalination*, vol. 312, pp. 2-9,

[20] I. L. Alsvik and M. B. Hagg. 2013. Preparation of Thin Film Composite Membranes with Polyamide Film on Hydrophilic Supports. *Journal of Membrane Science*, vol. 428, pp. 225-231.

[21] N.-N. Bui and J. McCutcheon. 2013. Hydrophilic Nanofibers as New Supports for Thin Film Composite Membranes for Engineered Osmosis. *Environmental Science & Technology*, April 1, 2013.

[22] L. A. Hoover, J. D. Schiffman, and M. Elimelech. 2013. Nanofibers in Thin-Film Composite Membrane Support Layers: Enabling Expanded Application of Foward and Pressure Retarded Osmosis. *Desalination*, vol. 308, pp. 73-81.

[23] A. D. Khawaji, I. K. Kutubkhanah, and J. M. Wie. 2008. Advances in Seawater Desalination Technologies. *Desalination,* vol. 221, pp. 47-69.

[24] R. Semiat. 2008. Energy Issues in Desalination Processes. *Environmental Science and Technology,* vol. 42, pp. 8193-8201.

[25] R. L. Stover. 2007. Seawater Reverse Osmosis with Isobaric Energy Recovery Devices. *Desalination,* vol. 203, pp. 168-175.

[26] T. F. Seacord, S. D. Coker, and J. MacHarg. 2005. Affordable Desalination Collaboration 2005 Results, *Desalination & Water Reuse,* pp. 10-22.

[27] J. P. MacHarg. 2002. Retro-Fitting Existing SWRO Systems with a New Energy Recovery Device. *Desalination,* vol. 153, pp. 253-264.

[28] A. J. Morton, I. K. Callister, and N. M. Wade. 1996. Environmental Impacts of seawater Distillation and Reverse Osmosis Processes. *Desalination,* vol. 108, pp. 1-10.

[29] D. A. Roberts, E. L. Johnston, and N. A. Knott. 2010. Impacts of Desalination Plant Discharges on the Marine Environment: A Critical Review of Published Studies. *Water Research,* vol. 44, pp. 5117-5128.

[30] S. Lattemann and T. Hopner. 2008. Environmental Impact and Impact Assessment of Seawater Desalination. *Desalination,* vol. 220, pp. 1-15.

[31] I. Safrai and A. Zask. 2008. Reverse Osmosis Desalination Plants — Marine Environmentalist Regulator Point of View. *Desalination,* vol. 220, pp. 72-84.

[32] E. Gacia, O. Invers, M. Manzanera, E. Ballesteros, and J. Romero. 2007. Impact of the Brine from a Desalination Plant on a Shallow Seagress (*Posidonia oceanica*) Meadow. *Estuarine Coastal and Shelf Science,* vol. 72, pp. 579-590.

[33] H. Baalousha. 2006. Desalination Status in the Gaza Strip and Its Environmental Impact. *Desalination,* vol. 196, pp. 1-12.

[34] R. Einav, K. Harussi, and D. Perry. 2002. The Footprint of the Desalination Processes on the Environment. *Desalination,* vol. 152, pp. 141-154.

[35] Y. Fernandez-Torquemada, J. L. sanchez-Lizaso, and J. M. Gonzalez-Correa. 2005. Preliminary Results of the Monitoring of the Brine Discharge Produced by the SWRO Desalination Plant of Alicante (SE Spain). *Desalination,* vol. 182, pp. 395-402.

[36] K. Saito, M. Irie, S. Zaitsu, H. Sakai, H. Hayashi, and A. Tanioka. 2012. Power Generation with Salinity Gradient by Pressure Retarded Osmosis Using Concentrated Brine from SWRO System and Treated Sewage as Pure Water. *Desalination and Water Treatment,* vol. 41.

[37] A. Achilli, J. L. Prante, and A. E. Childress. 2013. Experimental Results of Pilot-scale RO-PRO System for Low Energy Desalination. University of Souther California.

[38] A. Achilli, T. Y. Cath, E. A. Marchand, and A. E. Childress. 2009. Harvesting Energy from Wastewater with Pressure Retarded Osmosis. *24th Annual Water Reuse Symposium*, Seattle, WA,

[39] A. Zhu, P. D. Christofides, and Y. Cohen. 2009. Minimization of Energy Consumption for a Two-Pass Membrane Desalination: Effect of Energy Recovery, Membrane Rejection, and Retentate Recycling. *Journal of Membrane Science*, pp. 126-137.

[40] K. S. Spiegler and Y. M. El-sayed. 2001. The Energetics of desalination Processes. *Desalination,* vol. 134, pp. 109-128.

[41] M. Elimelech and W. A. Phillip. 2011. The Future of Seawater Desalination: Energy, Technology, and the Environment. *Science,* vol. 333, pp. 712-717.

[42] B. Sauvet-Goichon. 2007. Ashkelon Desalination Plant — A Successful Challenge. *Desalination,* vol. 203, pp. 75-81.

[43] V. G. Molina, M. Taub, L. Yohay, and M. Busch. 2011. Long Term Membrane Process and Performance in Ashkelon Seawater Reverse Osmosis Desalination Plant. *Desalination and Water Treatment,* vol. 31, pp. 115-120,

[44] A. Achilli and A. E. Childress. 2010. Pressure Retarded Osmosis: From the Vision of Sidney Loeb to the First Prototype Installation — Review. *Desalination,* vol. 261, pp. 205-211.

[45] N. Y. Yip and M. Elimelech. 2012. Thermodynamic and Energy Efficiency Analysis of Power Generation from Natural Salinity Gradients by Pressure Retarded Osmosis. *Environmental Science & Technology,* vol. 46, pp. 5230-5239.

[46] B. E. Logan and M. Elimelech. 2012. Membrane-Based Processes for Sustainable Power Generation Using Water. *Nature,* vol. 488, pp. 313-319,

[47] A. Achilli, T. Y. Cath, and A. E. Childress. 2009. Power Generation with Pressure Retarded Osmosis: An Experimental and Theoretical Investigation. *Journal of Membrane Science,* vol. 343 pp. 42-52.

[48] N. Y. Yip, A. Tiraferri, W. A. Phillip, J. D. Schiffman, L. A. Hoover, Y. C. Kim. 2011. Thin-Film Composite Pressure Retarded Osmosis Membranes for Sustainable Power Generation from Salinity Gradients. *Environmental Science & Technology,* vol. 45, pp. 4360-4369.

[49] J. R. McCutcheon and M. Elimelech. 2006. Influence of Concentrative and Dilutive Internal Concentration Polarization on Flux Behavior in Forward Osmosis. *Journal of Membrane Science,* vol. 284, pp. 237-247.

[50] G. Schock and A. Miguel. 1987. Mass Transfer and Pressure Loss in Spiral Wound Modules. *Desalination,* vol. 64, pp. 339-352.

[51] D. V. Gauwbergen and J. Baeyens. 1997. Macroscopic Fluid Flow Conditions in Spiral-Wound Membrane Elements. *Desalination,* vol. 110, pp. 287-299.

[52] University of Nevada, 2011. Hydration Technology Innovations (HTI). University of Nevada, Reno, Nevada.

[53] C. P. Koutsou, S. G. Yiantsios, and A. J. Karabelas. 2007. Direct Numerical Simulation of Flow In Spacer-Filled Channels: Effect of Spacer Geometrical Characteristics. *Journal of Membrane Science,* vol. 291, pp. 53-69.

[54] C. P. Koutsou, S. G. Yiantsios, and A. J. Karabelas. 2009. A Numerical and Experimental Study of Mass Transfer in Spacer-Filled Channels: Effects of Spacer Geometrical Characteristics and Schmidt Number. *Journal of Membrane Science,* vol. 326, pp. 234-251.

[55] A. Zhu, P. D. Christofides, and Y. Cohen. 2009. Minimization of Energy Consumption for a Two-Pass Membrane Desalination: Effect of Energy Recovery, Membrane Rejection and Retentate Recycling. *Journal of Membrane Science,* vol. 339, pp. 126-13.

[56] K. P. Lee, T. C. Arnot, and D. Mattia. 2011. A Review of Reverse Osmosis Membrane Materials for Desalination-Development To Date and Future Potential. *Journal of Membrane Science,* vol. 370, pp. 1-22.

[57] M. Shannon, P. Bohn, M. Elimelech, J. Georgiadis, B. Marinas, and A. Mayes. 2008. Science and Technology for Water Purification in the Coming Decades. *Nature,* vol. 452, pp. 301-310.

[58] Y. C. Kim, Y. Kim, D. Oh, and K. H. Lee. 2013. Experimental Investigation of a Spiral-Wound Pressure-Retarded Osmosis Membrane Module for Osmotic Power Generation. *Environmental Science & Technology,* vol. 47, pp. 2966-2973.

[59] S. E. Skilhagen. 2010. Osmotic Power — A New, Renewable Energy Source. *Desalination and Water Treatment,* vol. 15, pp. 271-278.

[60] A. Zhu, P. D. Christofides, and Y. Cohen. 2009. Effect of Thermodynamic Restriction on Energy Cost Optimization of RO Membrane Water Desalination. *Industrial & Engineering Chemistry Research,* vol. 48, pp. 6010-6021,

[61] C. Doyle. 2012. Apple to Build 20 MW Solar Farm at North Carolina Data Centre. http://www.siliconrepublic.com/start-ups/item/25892-apple-to-build-20mw-solar/ percentC2percentA0http://images.apple.com/environment/reports/docs/Apple_Facilities_Report_2012.pdf

[62] P. Denholm, M. Hand, M. Jackson, and S. Ong. 2009. Land-Use Requirements of Modern Wind Power Plants in the United States. National Renewable Energy Laboratory (NREL) Golden, CO.

APPENDICES

A Specific RO Alone Experimental Flowrates, Pressures, and Concentrations

B Specific RO-PX Experimental Flowrates, Pressures, and Concentrations

C Specific RO-PRO Experimental Flowrates, Pressures, and Concentrations

APPENDIX A

Specific RO Alone Experimental Flowrates, Pressures, and Concentrations

Table A1.—RO Alone Experimental Flowrates, Pressures, and Concentrations for 20% RO Recovery

	Flowrate (LPM)	Pressure (psi)	Concentration (g/L)
RO Feed	5.0	543	35.0
RO Permeate	1.0	-	1.2
RO Brine/System Exit	4.0	528	42.4

Table A2.—RO Alone Experimental Flowrates, Pressures, and Concentrations for 30% RO Recovery

	Flowrate (LPM)	Pressure (psi)	Concentration (g/L)
RO Feed	5.0	658	35.0
RO Permeate	1.5	-	0.9
RO Brine/System Exit	3.5	644	48.9

APPENDIX B

Specific RO-PX Experimental Flowrates, Pressures, and Concentrations

Table B1.—RO-PX Experimental Flowrates, Pressures, and Concentrations for 20% RO recovery

	Flowrate (LPM)	Pressure (psi)	Concentration (g/L)
System In	5.0	28	35.2
PX Low In	2.5	28	35.2
RO Pump In	2.5	28	35.2
PX High Out	2.0	515	34.6
RO Feed	4.5	560	34.6
RO Permeate	1.0	-	1.2
RO Brine/PX High In	3.5	530	40.2
PX Low Out/System Out	4.0	5	41.0

Table B2.—RO-PX Experimental Flowrates, Pressures, and Concentrations for 30% RO Recovery

	Flowrate (LPM)	Pressure (psi)	Concentration (g/L)
System In	5.0	24	35.1
PX Low In	2.0	24	35.1
RO Pump In	3.0	24	35.1
PX High Out	2.0	612	37.6
RO Feed	5.0	659	37.6
RO Permeate	1.5	-	0.9
RO Brine/PX High In	3.5	625	45.9
PX Low Out/System Out	3.5	5	46.4

APPENDIX C

Specific RO-PRO Experimental Flowrates, Pressures, and Concentrations

Table C1.—Average RO-PRO experimental Flowrates, Pressures, and Concentrations for 20% RO Recovery and 100 psi Draw Solution Entering Pressure

	Flowrate (LPM)	Pressure (psi)	Concentration (g/L)
System In	5.0 +/- 0.0	48 +/- 1	35.0 +/- 0.7
PX Low In	4.2 +/- 0.2	48 +/- 1	35.0 +/- 0.7
RO Pump In	0.8 +/- 0.2	48 +/- 1	35.0 +/- 0.7
PX High Out	4.9 +/- 0.1	78 +/- 5	33.2 +/- 0.6
RO Feed	5.8 +/- 0.2	542 +/- 13	33.2 +/- 0.6
RO Permeate	1.0 +/- 0.0	-	-
RO Brine	4.8 +/- 0.2	522 +/- 14	39.9 +/- 1.2
$PRO_{DS,en}$	4.8 +/- 0.2	100 +/- 4	39.9 +/- 1.2
PRO Permeate	0.9 +/- 0.1	-	-
$PRO_{DS,ex}$/PX High In	5.7 +/- 0.2	93 +/- 5	32.4 +/- 0.8
$PRO_{F,en}$	5.0 +/- 0.0	17 +/- 2	-
$PRO_{F,ex}$	4.1 +/- 0.2	8 +/- 1	-
PX Low Out/System Out	5.0 +/- 0.0	8 +/- 1	32.4 +/- 0.8

Table C2.—Average RO-PRO Experimental Flowrates, Pressures, and Concentrations for 20% RO Recovery and 150 psi Draw Solution Entering Pressure

	Flowrate (LPM)	Pressure (psi)	Concentration (g/L)
System In	5.0 +/- 0.0	45 +/- 2	34.9 +/- 0.7
PX Low In	4.1 +/- 0.3	45 +/- 2	34.9 +/- 0.7
RO Pump In	0.9 +/- 0.3	45 +/- 2	34.9 +/- 0.7
PX High Out	4.8 +/- 0.2	137 +/- 5	33.2 +/- 0.6
RO Feed	5.6 +/- 0.2	543 +/- 13	33.3 +/- 0.7
RO Permeate	1.0 +/- 0.0	-	-
RO Brine	4.6 +/- 0.1	523 +/- 14	39.6 +/- 0.9
$PRO_{DS,en}$	4.6 +/- 0.1	155 +/- 4	39.6 +/- 0.9
PRO Permeate	0.6 +/- 0.1	-	-
$PRO_{DS,ex}$/PX High In	5.2 +/- 0.1	152 +/- 4	33.3 +/- 0.7
$PRO_{F,en}$	5.0 +/- 0.0	20 +/- 3	-
$PRO_{F,ex}$	4.4 +/- 0.1	9 +/- 1	-
PX Low Out/System Out	4.8 +/- 0.2	7 +/- 1	33.3 +/- 0.8

Table C3.—Average RO-PRO Experimental Flowrates, Pressures, and Concentrations for 20% RO Recovery and 200 psi Draw Solution Entering Pressure

	Flowrate (LPM)	Pressure (psi)	Concentration (g/L)
System In	5.0 +/- 0.0	41 +/- 1	35.0 +/- 0.7
PX Low In	4.0 +/- 0.0	41 +/- 1	35.0 +/- 0.7
RO Pump In	1.0 +/- 0.0	41 +/- 1	35.0 +/- 0.7
PX High Out	4.4 +/- 0.1	185 +/- 6	33.2 +/- 0.6
RO Feed	5.4 +/- 0.1	542 +/- 7	33.2 +/- 0.6
RO Permeate	1.0 +/- 0.0	-	-
RO Brine	4.4 +/- 0.1	520 +/- 7	39.9 +/- 1.2
$PRO_{DS,en}$	4.4 +/- 0.1	202 +/- 6	39.9 +/- 1.2
PRO Permeate	0.4 +/- 0.1	-	-
$PRO_{DS,ex}$/PX High In	4.6 +/- 0.6	199 +/- 5	32.4 +/- 0.8
$PRO_{F,en}$	5.0 +/- 0.0	26 +/- 3	-
$PRO_{F,ex}$	4.6 +/- 0.1	10 +/- 0	-
PX Low Out/System Out	4.4 +/- 0.1	7 +/- 1	32.4 +/- 0.8

Table C4.—Average RO-PRO Experimental Flowrates, Pressures, and Concentrations for 20% RO Recovery and 250 psi Draw Solution Entering Pressure

	Flowrate (LPM)	Pressure (psi)	Concentration (g/L)
System In	5.0 +/- 0.0	38 +/- 2	35.0 +/- 0.5
PX Low In	4.0 +/- 0.0	38 +/- 2	35.0 +/- 0.5
RO Pump In	1.0 +/- 0.0	38 +/- 2	35.0 +/- 0.5
PX High Out	4.2 +/- 0.1	236 +/- 2	34.3 +/- 0.4
RO Feed	5.2 +/- 0.1	552 +/- 10	34.3 +/- 0.4
RO Permeate	1.0 +/- 0.0	-	-
RO Brine	4.2 +/- 0.1	528 +/- 11	40.0 +/- 0.6
$PRO_{DS,en}$	4.2 +/- 0.1	250 +/- 0	40.0 +/- 0.6
PRO Permeate	0.2 +/- 0.1	-	-
$PRO_{DS,ex}$/PX High In	4.4 +/- 0.1	251 +/- 1	36.1 +/- 0.6
$PRO_{F,en}$	5.0 +/- 0.0	38 +/- 6	-
$PRO_{F,ex}$	4.8 +/- 0.1	14 +/- 6	-
PX Low Out/System Out	4.2 +/- 0.1	7 +/- 1	36.0 +/- 0.6

Table C5.—Average RO-PRO Experimental Flowrates, Pressures, and Concentrations for 30% RO Recovery and 100 psi Draw Solution Entering Pressure

	Flowrate (LPM)	Pressure (psi)	Concentration (g/L)
System In	5.0 +/- 0.0	41 +/- 3	35.4 +/- 0.4
PX Low In	4.0 +/- 0.0	41 +/- 3	35.4 +/- 0.4
RO Pump In	1.0 +/- 0.0	41 +/- 3	35.4 +/- 0.4
PX High Out	4.3 +/- 0.2	85 +/- 5	34.6 +/- 0.5
RO Feed	5.3 +/- 0.2	635 +/- 10	34.6 +/- 0.8
RO Permeate	1.5 +/- 0.0	-	-
RO Brine	3.8 +/- 0.2	616 +/- 10	45.3 +/- 0.7
$PRO_{DS,en}$	3.8 +/- 0.2	105 +/- 4	45.3 +/- 0.7
PRO Permeate	0.9 +/- 0.1	-	-
$PRO_{DS,ex}$/PX High In	4.8 +/- 0.4	99 +/- 6	35.8 +/- 1.0
$PRO_{F,en}$	5.0 +/- 0.0	17 +/- 2	-
$PRO_{F,ex}$	4.1 +/- 0.1	8 +/- 1	-
PX Low Out/System Out	4.3 +/- 0.2	6 +/- 1	35.6 +/- 1.2

Table C6.—Average RO-PRO Experimental Flowrates, Pressures, and Concentrations for 30% RO Recovery and 150 psi Draw Solution Entering Pressure

	Flowrate (LPM)	Pressure (psi)	Concentration (g/L)
System In	5.0 +/- 0.0	38 +/- 2	35.8 +/- 0.5
PX Low In	3.9 +/- 0.3	38 +/- 2	35.8 +/- 0.5
RO Pump In	1.1 +/- 0.3	38 +/- 2	35.8 +/- 0.5
PX High Out	4.2 +/- 0.2	141 +/- 3	35.3 +/- 0.3
RO Feed	5.3 +/- 0.2	646 +/- 5	34.9 +/- 1.7
RO Permeate	1.5 +/- 0.0	-	-
RO Brine	3.8 +/- 0.2	624 +/- 5	45.6 +/- 0.5
$PRO_{DS,en}$	3.8 +/- 0.2	157 +/- 3	45.6 +/- 0.5
PRO Permeate	0.6 +/- 0.1	-	-
$PRO_{DS,ex}$/PX High In	4.4 +/- 0.2	155 +/- 3	37.5 +/- 1.0
$PRO_{F,en}$	5.0 +/- 0.0	22 +/- 2	-
$PRO_{F,ex}$	4.4 +/- 0.1	10 +/- 1	-
PX Low Out/System Out	4.1 +/- 0.1	6 +/- 1	37.1 +/- 1.5

Table C7.—Average RO-PRO Experimental Flowrates, Pressures, and Concentrations for 30% RO Recovery and 200 psi Draw Solution Entering Pressure

	Flowrate (LPM)	Pressure (psi)	Concentration (g/L)
System In	5.0 +/- 0.0	35 +/- 4	36.4 +/- 0.4
PX Low In	3.7 +/- 0.4	35 +/- 4	36.4 +/- 0.4
RO Pump In	1.3 +/- 0.4	35 +/- 4	36.4 +/- 0.4
PX High Out	4.0 +/- 0.0	188 +/- 4	36.4 +/- 0.5
RO Feed	5.4 +/- 0.3	660 +/- 10	36.4 +/- 0.8
RO Permeate	1.5 +/- 0.0	-	-
RO Brine	3.9 +/- 0.3	639 +/- 10	46.3 +/- 0.8
$PRO_{DS,en}$	3.9 +/- 0.3	204 +/- 4	46.3 +/- 0.8
PRO Permeate	0.4 +/- 0.1	-	-
$PRO_{DS,ex}$/PX High In	4.3 +/- 0.4	203 +/- 4	39.4 +/- 1.3
$PRO_{F,en}$	5.0 +/- 0.0	28 +/- 4	-
$PRO_{F,ex}$	4.5 +/- 0.3	10 +/- 0	-
PX Low Out/System Out	4.0 +/- 0.0	6 +/- 1	39.5 +/- 1.3

Table C8.—Average RO-PRO Experimental Flowrates, Pressures, and Concentrations for 30% RO Recovery and 250 psi Draw Solution Entering Pressure

	Flowrate (LPM)	Pressure (psi)	Concentration (g/L)
System In	5.0 +/- 0.0	35 +/- 3	36.5 +/- 0.9
PX Low In	3.3 +/- 0.5	35 +/- 3	36.5 +/- 0.9
RO Pump In	1.8 +/- 0.5	35 +/- 3	36.5 +/- 0.9
PX High Out	4.0 +/- 0.0	240 +/- 6	37.1 +/- 0.7
RO Feed	5.8 +/- 0.5	661 +/- 14	36.5 +/- 1.2
RO Permeate	1.5 +/- 0.0	-	-
RO Brine	4.2 +/- 0.5	637 +/- 15	46.2 +/- 1.1
$PRO_{DS,en}$	4.2 +/- 0.5	253 +/- 5	46.2 +/- 1.1
PRO Permeate	0.3 +/- 0.2	-	-
$PRO_{DS,ex}$/PX High In	4.8 +/- 0.2	251 +/- 11	41.0 +/- 0.7
$PRO_{F,en}$	5.0 +/- 0.0	41 +/- 8	-
$PRO_{F,ex}$	4.7 +/- 0.2	11 +/- 1	-
PX Low Out/System Out	4.0 +/- 0.0	6 +/- 1	40.9 +/- 0.7